The Astrophysical Journal, 711:268–283, 2010 March 1 doi:10.1088/0004-637X/711/1/268

FEEDBACK FROM CENTRAL BLACK HOLES IN ELLIPTICAL GALAXIES. II. CAN PURELY MECHANICAL ENERGY FEEDBACK MODELS WORK?

Min-Su Shin[1], Jeremiah P. Ostriker[1,2], and Luca Ciotti[3]
[1] Princeton University Observatory, Peyton Hall, Princeton, NJ 08544-1001, USA
[2] Institute of Astronomy, University of Cambridge, Madingley Road, Cambridge CB3 0HA, UK
[3] Department of Astronomy, University of Bologna, via Ranzani 1, I-40127, Bologna, Italy
Received 2009 May 27; accepted 2010 January 20; published 2010 February 9

ABSTRACT

By using high-resolution one-dimensional hydrodynamical simulations, we investigate the effects of purely mechanical feedback from super massive black holes (SMBHs) in the evolution of elliptical galaxies for a broad range of feedback efficiencies and compare the results to four major observational constraints. In particular, we focus on (1) the central black hole to stellar mass ratio of the host galaxy, (2) the lifetime of the luminous quasar phase, (3) the mass of stars formed in the host galaxy within the last Gyr, and (4) the X-ray luminosity of the hot diffuse gas. As a result, we try to pin down the most successful range of mechanical feedback efficiencies. We find that while low feedback efficiencies result in too much growth of the SMBH, high efficiencies totally blow out the hot interstellar gas, and the models are characterized by very low thermal X-ray luminosity well below the observed range. The net lifetime of the quasar phase is strongly coupled to the mass ratio between SMBH and its host galaxy, while the X-ray luminosity is generally correlated to the recent star formation within the last Gyr. When considering the popularly adopted model of the constant feedback efficiency, the feedback energy deposited into the ambient medium should be more than 0.01% of the SMBH accretion energy to be consistent with the SMBH mass to stellar mass ratio in the local universe. Yet, the X-ray luminosity of the hot gas favors about 0.005% of the accretion energy as the mechanical active galactic nucleus (AGN) feedback energy. We conclude that the purely mechanical feedback mode is unlikely to be simultaneously compatible with all four observable tests, even allowing a broad range of feedback efficiencies, and that including both radiative and mechanical feedback together may be a solution to comply with the observational constraints. In addition to the adopted observational constraints, our simulations also show that the ratio of SMBH growth rate over its current mass and the density and temperature distribution of hot gas can be useful observable diagnostics for AGN feedback efficiencies.

Key words: galaxies: active – galaxies: evolution – galaxies: formation – galaxies: nuclei – methods: numerical

1. INTRODUCTION

The well-established empirical correlations between the mass of supermassive black holes (SMBHs) and several properties of their host galaxies are providing new insights and also new problems for our understanding of massive galaxy evolution. In particular, the more massive SMBHs are hosted in the more massive bulges, galaxies, and dark matter halos (Kormendy & Richstone 1995; Magorrian et al. 1998; Ferrarese & Merritt 2000; Gebhardt et al. 2000; Ferrarese 2002; Yu & Tremaine 2002; Marconi & Hunt 2003; Häring & Rix 2004), and the shape of the light profile is related to the mass of the central SMBH (e.g., Graham et al. 2001). Moreover, the co-evolution of SMBHs and host galaxies is also supported by the observational evidence of the proportionality between the galaxy star formation rate (SFR) and the mass accretion rate of the SMBHs over a broad range of redshifts (e.g., Boyle & Terlevich 1998; Haiman et al. 2004; Miller 2007; Shankar et al. 2009).

This tight correlation between the stellar mass of the host spheroid and the SMBH mass has been tackled by various theoretical explanations that are based on self-regulation processes of feedback effects from the accreting SMBHs. When SMBHs are in an active phase (i.e., active galactic nucleus, AGN), feedback via either the mass ejection by winds or jets, or alternatively the emitted radiation, regulates the mass accretion rate and the final SMBH mass (Rees 1984; Krolik 1999; Heckman 2009). The feedback can be in the forms of radiatively or mechanically driven winds (e.g., Silk & Rees 1998; Fabian 1999; King & Pounds 2003; Granato et al. 2004; King 2005; Murray et al. 2005; Fabian et al. 2006), of a turbulent energy transportation near the SMBHs (e.g., Begelman & Nath 2005), of radiative effects such as photoionization and Compton heating (e.g., Sazonov et al. 2005; Ciotti & Ostriker 2007), or of a blast wave (e.g., Menci et al. 2008).

The idea of feedback from SMBHs also has given rise to various hypotheses that could answer important open questions in galaxy and galaxy cluster evolution. For example, significant star formation can be prevented by energy deposited from AGNs, which suppresses the supply of cold gas, and the further late star formation after the bulk of stars form early (e.g., Croton et al. 2006; Cattaneo et al. 2007, 2009; Khalatyan et al. 2008; Kormendy et al. 2009) and transforms blue star-forming galaxies to red galaxies (e.g., Lagos et al. 2008). The AGN feedback may help us explain galaxy downsizing by making the AGN feedback processes depend on the mass of dark matter halo (e.g., Scannapieco et al. 2005). Moreover, the feedback may alter energy and mass distribution of intergalactic medium in galaxy clusters (Cavaliere et al. 2002; Scannapieco & Oh 2004; Scannapieco et al. 2005; Thacker et al. 2006; Chandran & Rasera 2007; Chatterjee et al. 2008).

Independently of the specific model considered, the problem of the self-regulated growth of SMBHs and spheroids can be summarized as two questions about effects from AGN feedback. First, self-regulation requires that feedback effects have to be well-timed responding to the growth of stellar mass. Suppose that there is a long time-lag either between the start of star formation and the onset of AGN feedback, or between the beginning of the feedback effects and heating surrounding

gas, then the pace of star formation can be faster than the growth of SMBHs. This case would weaken the tight correlation between SMBH mass and bulge mass. Therefore, this timing problem is closely relevant to how SMBHs are fueled and when they ignite AGN feedback (Cavaliere et al. 1983; Shull 1983; Shlosman et al. 1990; Quataert & Narayan 2000; Kawaguchi 2003; Narayan & Quataert 2005; Tan & Blackman 2005; Jogee 2006; Königl 2006; Davies et al. 2007; Müller Sánchez et al. 2009). Second, the impact of AGN feedback on host galaxies of SMBHs depends on how the gravitational accretion energy is converted to outflowing mass and radiation from SMBHs, and is transported to the surrounding medium (King 2003; Proga 2005, 2007; Murray et al. 2005; Proga et al. 2008; Hardee 2008). In some circumstances, the energy conversion might even cause the enhancement of star formation instead of suppressing star formation by allowing shock-induced star formation (e.g., Silk 2005; Ciotti & Ostriker 2007; Pipino et al. 2009). Very efficient energy output and conversion will tend to inhibit the SMBH growth overly, and very inefficient coupling of the outflowing energy to the ambient gas would lead to SMBHs more massive even than those observed. This energy conversion problem coupled to the timing problem determines the efficiency of AGN feedback and the final properties of SMBHs and their host galaxies.

Therefore, the proper understanding of the timing problem and the energy conversion problem is critical to understand physics of AGN feedback in detail. As Elvis (2006) emphasizes, the structure and physics of AGNs are entangled together, and it is difficult to find a direct connection between feedback from AGNs and other properties of galaxies without elucidating the complicated connection of feedback effects onto the host galaxies. Even though we can begin to ask questions related to AGN feedback on a large scale such as galaxy mergers, galaxy clusters, and cosmological evolution by using simple descriptions of feedback (Cattaneo et al. 2005; Hopkins et al. 2005; Kawata & Gibson 2005; Thacker et al. 2006; Monaco et al. 2007; Menci et al. 2008; Khalatyan et al. 2008), we cannot simplify the complex physics entangling the SMBHs and their host galaxies without the better understanding of involved physics, ranging from the small-scale physics of AGNs to the larger-scale physics of galaxies (Blandford 2001).

In the literature, feedback has been mainly considered in two aspects: radiative feedback and mechanical feedback. Radiative feedback is a consequence of radiative heating and radiation pressure by a strong radiation from AGNs, including photoionization and Compton heating (Ciotti & Ostriker 2001; Sazonov et al. 2004, 2005; Fabian et al. 2006; Ciotti & Ostriker 2007). And computing the effects of radiative feedback is straightforward since we directly observe the hard radiation from AGNs that causes the ambient heating: there are few uncertainties in computing this type of feedback. Yet, mechanical feedback is associated to winds and jets from accreting SMBHs (Tabor & Binney 1993; Binney & Tabor 1995; Friaca & Terlevich 1998; Veilleux et al. 2005; Springel et al. 2005a; Königl 2006), and it can be very important although the strength of the effects is highly uncertain. Both feedback modes increase the internal energy of the interstellar medium (ISM) and may cause local and/or global outflows. But their properties and efficiencies are different because radiative feedback (in an optically thin medium) acts almost instantaneously, and is transported without mass loading over the entire galaxy. By any accounting the radiative energy emitted by the accreting SMBH exceeds the emitted mechanical energy; but radiative feedback couples to the ambient medium far less effectively. So there is a trade-off in the effectiveness of the two types of feedback that must be investigated in detail.

In this paper, we extend the analysis of the purely mechanical feedback models described in Ciotti et al. (2009b, hereafter Paper I), by comparing the results of simulations with different feedback efficiencies against four well-constrained observational properties of local elliptical galaxies and their SMBHs. In Paper I, new hydrodynamical evolutionary models, combining radiative and mechanical feedback, have been developed from the previous purely radiative models (Ciotti & Ostriker 1997, 2001, 2007). In particular, it has been found that purely mechanical feedback models may not be the complete description of AGN feedback in Paper I. Though both feedback modes can be important together, first we ask in more detail whether popularly used purely mechanical feedback models can be accepted to explain important properties of SMBHs and their host galaxies in more detail. In practice, (1) as most commonly tested in previous research, we estimate the evolution of the ratio between the SMBH mass and the host galaxy stellar mass. This ratio has been a key diagnosis to test the formation theory of bulge-dominated galaxies since the correlation between two masses is found to be tight in observations. (2) The lifetime of the luminous quasar phase in the models is also compared to the observationally estimated lifetime (or duty cycle[4]; see Martini 2004 for a discussion). These two constraints are mainly governed by a small-scale physics around SMBHs. (3) Another useful probe of the growing stellar mass in elliptical galaxies is the amount of the recently formed stellar mass, which is well constrained by observations in the rest-frame UV (see Yi et al. 2007 and Kaviraj et al. 2007 for a discussion). (4) We finally compare the X-ray thermal luminosity of diffuse hot gas in the models with the luminosity observed for local elliptical galaxies (see Pope 2009 for a discussion). If the assumed AGN feedback produces effects which are not consistent with these observational tests, we may have to reconsider the adopted AGN feedback models and their effects in galaxy evolution.

We investigate how the four observational tests can be used to constrain the AGN feedback models, and how the self-regulation process works depending on the adopted models. If there is an appropriate efficiency of the mechanical AGN feedback and it is the only possible mode of feedback, then the purely mechanical feedback model must be consistent with the four observational constraints. In other words, if any values of the feedback efficiency cannot produce acceptable simulation results, we may need to consider the more general possibility which includes both radiative feedback and mechanical feedback modes, as hinted in Paper I. We also suggest various observable diagnostics which are related to the physics of AGN feedback, and which can be used to narrow down the feedback models and their efficiency, in addition to the four main tests listed above.

This paper is organized as follows. In Section 2, we summarize the main components of two purely mechanical feedback models adopted for the simulations. In Sections 3 and 4. we present the general properties of simulation results, and comparisons between models and observational constraints are given for a broad range of feedback efficiencies. Other possible tests

[4] The duty cycle is commonly defined as the fraction of time on AGN phase with luminosity weights (e.g., Ciotti & Ostriker 2001). But the net lifetime in this paper is simply defined by the net duration of AGN with luminosity above some limit. Therefore, the net lifetime used in this paper can be slightly different from the luminosity-weighted AGN duty cycle multiplied by the Hubble time.

are suggested in Section 5, while the main results are summarized and discussed in Section 6.

2. MODELS

2.1. Simulation Setup

Here, we summarize the main properties of the purely mechanical feedback models, which are described in detail in Paper I. In the Appendix, we summarize the important input physics such as mass losses from evolving stars, the various timescales of the problem, and the treatment of the purely mechanical and purely radiative feedback; in the present section only the formulae required for the discussion are given.

In accordance to several observational constraints, at the beginning of the simulation, the galaxy model is described by a spherically symmetric Jaffe model for stellar mass (Jaffe 1983), which is immersed in a dark matter halo, so that the total mass density follows a r^{-2} profile (Ciotti et al. 2009a). The effective radius of the stellar mass distribution R_e is about 6.91 kpc, and the line-of-sight central velocity dispersion is 260 km s^{-1}. The total stellar mass M_* is $2.87 \times 10^{11}\ M_\odot$, and inside the half-mass stellar radius the stellar-to-dark matter mass ratio is fixed to unity. The obtained galaxy model obeys the observed Faber–Jackson relation and the fundamental plane of local ellipticals. In all models, the initial galaxy model has the central SMBH with the mass $M_{\rm BH} = 0.001\ M_*$, approximately following the Magorrian et al. (1998) relationship. This assumption is further discussed in Section 6.

We simulate the evolution of gas by solving Eulerian equations of hydrodynamics with appropriate mass, momentum, and energy sources (see the Appendix). All calculations are conducted with a one-dimensional logarithmic radial grid extending from 2.5 pc to 200 kpc which has 120 bins. The simulation begins at 2 Gyr, i.e., a redshift of $z \sim 3.2$ for the LCDM cosmology with $\Omega_{\rm m} = 0.3$, $\Omega_\lambda = 0.7$, and $H_0 = 70$ km s^{-1} Mpc^{-1}, and continues until 14 Gyr. We note that the bulk of the mass of elliptical galaxies is already in place at our starting epoch. A variety of heating and cooling processes are included as well as spherically symmetric radiative transfer in several bands treated in the Eddington approximation.

We remark that, as in the previous papers (Ciotti & Ostriker 2001, 2007) and Paper I, the galaxy model is initially devoid of gas, and has an outflow boundary condition for the last radial grid point. Consequently, the ISM is solely provided by the recycled gas produced via stellar evolution, and the confining effect of the intergalactic medium is not considered. For these reasons, the obtained X-ray luminosity should be considered as a lower limit of the observed values (see Pellegrini et al. 2009).

We simulate an isolated elliptical galaxy where the evolution of gas is not affected by any cosmological effects such as galaxy mergers and satellite accretions (Hopkins et al. 2008) or just cold gas accretion (Khalatyan et al. 2008). The probability of mergers for our tested cases since 2 Gyr may be so small for the considered mass range that a passive evolution of the simulated elliptical galaxy is still valid (Maller et al. 2006; Kang et al. 2007; Drory & Alvarez 2008). Moreover, observations of nearby active merger remnants show that the local physical process around the central SMBH such as star formation on the nuclear disk and supernovae (SNe) is more important than what is simply described in galaxy merger simulations with AGN feedback (e.g., Tecza et al. 2000; Max et al. 2007, for NGC 6240), supporting the importance of our approach to include AGN feedback physics in detail. We also emphasize that the moderate-luminosity AGN activity at low redshift may not be caused by mergers even though a bright quasar phase may need mergers as triggers (Grogin et al. 2005; Li et al. 2008).

2.2. Physics of Purely Mechanical Feedback Models

As well known, there are four channels to change the total mass of gas in a galaxy.[5] First, winds from stars leaving the main sequence, giant stars, planetary nebulae, SNe, etc. contribute a significant amount of mass in gaseous form as the galaxy evolves: over the Hubble time, 10%–30% of the initial stellar mass is ejected by stars. Second, when the gas cools (for spherical models usually in a cold shell), star formation can occur, and then the newly formed stars will also contribute back gas with their mass losses. The third channel is accretion onto the central SMBH and the nuclear disk (Shlosman et al. 1990; Nulsen & Fabian 2000). In fact, cooled gas can form a circumnuclear disk around the SMBH (Tan et al. 2008), and then it can be used to form stars in circumnuclear starbursts. The fate of the remaining gas in the accretion disk is to produce radiation and finally being fed into the SMBH (Davies et al. 2007). In our simulations, we also model the secondary mass loss from circumnuclear stars, which also formed from recycled gas (i.e., mass loss and SNe) in our models, that contribute to the SMBH accretion (Shull 1983; Padovani & Matteucci 1993; Quataert 2004). Finally, the galactic gas can be blown out from the galaxy as a galactic wind/outflow.

Of direct interest for mechanical feedback models are the nuclear winds produced by the combined effects from the AGN energy output and the Type II SNe exploding in the star-forming circumnuclear disk. As assumed in Paper I, cold disks will form stars, and gas from the disks can be blown out by a strong wind from the central SMBH (Crenshaw et al. 2003; Krongold et al. 2008). In our prescription of the AGN wind loss, the mass-loss efficiency of the AGN wind η_w is defined to be the ratio of the disk outflow rate to the SMBH accretion rate. In Paper I, we introduced two different prescriptions:

$$\eta_{\rm w} = \begin{cases} 2, & \text{[A]} \\ \dfrac{3\eta_{\rm w}^{\rm M}}{4}\dfrac{l}{1+0.25l}, & \text{[B],} \end{cases} \tag{1}$$

where $l = L_{\rm BH}/L_{\rm Edd}$ is the bolometric luminosity $L_{\rm BH}$ of the central SMBH in Eddington units, and the maximum wind efficiency $\eta_{\rm w}^{\rm M}$ is related to the mechanical feedback efficiency (see Equation (3)). Therefore, as l increases up to 2 (see the Appendix), $\eta_{\rm w}$ approaches $\eta_{\rm w}^{\rm M}$ in the model of Type B.

In the purely mechanical feedback models, we include only the physics of mass, momentum, and energy transfer from the nuclear wind to the ISM (see Elvis 2000 for the description of the probable structure of a quasar), while the effect of a jet is not included. In particular, the mechanical energy output of the circumnuclear disk is modeled as

$$L_{\rm dw} = \epsilon_{\rm w}\dot{M}_{\rm BH}c^2 + \epsilon_{\rm II}c^2(1 - f_{\rm rem,h})\frac{M_{\rm dh*}}{\tau_{*\rm h}}, \tag{2}$$

where $\dot{M}_{\rm BH}$ and $M_{\rm dh*}/\tau_{*\rm h}$ are the growth rate of the SMBH mass and the SFR of massive stars in the disk, respectively (see the Appendix). In the second term of Equation (2), $\epsilon_{\rm II}$ and $f_{\rm rem,h}$ are the feedback efficiency by Type II SNe and the mass fraction

[5] Because our simulation does not consider galaxy mergers and (gas) accretion, a possible fifth channel of gas inflow is not included in the models as we already mentioned in Section 1.

Table 1
Efficiency Parameter of the Mechanical Feedback in the Both MA and MB Computed Models

Run	$\epsilon_{\rm w}^{\rm M}$	Run	$\epsilon_{\rm w}^{\rm M}$
1	1×10^{-5}	5	1×10^{-3}
2	5×10^{-5}	6	5×10^{-3}
3	1×10^{-4}	7	1×10^{-2}
4	5×10^{-4}	8	5×10^{-2}

of stellar remnants for high-mass stars, respectively. Therefore, when the SFR on the circumnuclear disk is high or the accretion rate to the SMBH is high, the total energy output from the disk wind is high with the contribution of the nuclear wind modulated by $\epsilon_{\rm w}$.

Our main concern in this paper is $\epsilon_{\rm w}$ which determines how efficiently the growing central SMBH can deposit the mechanical energy into its surrounding ISM. Following Paper I, we test two models:

$$\epsilon_{\rm w} \equiv \begin{cases} \epsilon_{\rm w}^{\rm M}, & \text{[A]} \\ \dfrac{3\epsilon_{\rm w}^{\rm M}}{4}\dfrac{l}{1+0.25l}, & \text{[B].} \end{cases} \quad (3)$$

In the both descriptions, $\eta_{\rm w}^{\rm M} = 1800\epsilon_{\rm w}^{\rm M}$ so that the velocity of the circumnuclear wind is about 10^4 km s^{-1} in accordance with observations of broad-line winds (Crenshaw et al. 2003).

In this paper, we maintain the nomenclature of Paper I, and we refer to purely mechanical feedback models of Type A and B as MA and MB models, respectively. It is finally important to recall that, even though radiative feedback effects are not considered in the simulations, $L_{\rm BH}$ has a fundamental importance in the MB models, as $\epsilon_{\rm w}$ is dependent of the luminosity.

The popular choice of $\epsilon_{\rm w}^{\rm M} = 0.005$ in Type A models has been adopted in the majority of previous research. For example, 0.5% of the accretion mass is immediately deposited to the ISM as a feedback energy, while assuming that 10% of the accreted mass is converted to radiation (Soltan 1982) in simulations of galaxy mergers (Springel et al. 2005a, 2005b; Hopkins et al. 2005; Johansson et al. 2009). Thacker et al. (2006) also examine a case that corresponds to our model A with $\epsilon_{\rm w}^{\rm M} = 0.005$, which easily heats up gas within a few Mpc. Other examples are found in investigations of the Sunyaev–Zel'dovich effect from quasars (e.g., Chatterjee et al. 2008; Scannapieco et al. 2008), downsizing of galaxy evolution (e.g., Scannapieco et al. 2005), the evolution of the black hole mass and bulge mass (e.g., Robertson et al. 2006), and the formation of elliptical galaxies (e.g., Khalatyan et al. 2008). However, ab initio we do not know of either an empirical basis for the adoption of this particular coefficient nor calculations from which it could be derived.

There have been some trials to pin down an acceptable range of $\epsilon_{\rm w}^{\rm M}$. For example, Scannapieco & Oh (2004) investigate the cases corresponding to the MA models with $\epsilon_{\rm w}^{\rm M} = 0.0025$ and 0.01, and conclude that the two values fail to explain quasar luminosity function and other structure formations. But as they note, $\epsilon_{\rm w}^{\rm M}$ is observationally not well constrained by their tests. Levine & Gnedin (2005) also examine how a constant mechanical feedback efficiency affects the distribution of AGN outflows by testing $\epsilon_{\rm w}^{\rm M} = 0.001$, 0.01, and 0.005. They find $\epsilon_{\rm w}^{\rm M} = 0.001$ as the best value by comparing their models with observationally derived filling fractions of AGN outflows. As these two examples show, the acceptable range of $\epsilon_{\rm w}^{\rm M}$ is still controversial for the MA models. However, the different purely mechanical models such as our MB models have not been tested extensively yet, even though they appear to be more close to the real AGN feedback process in which the feedback efficiency is expected to increase as one approaches the Eddington limit (Kurosawa & Proga 2009).

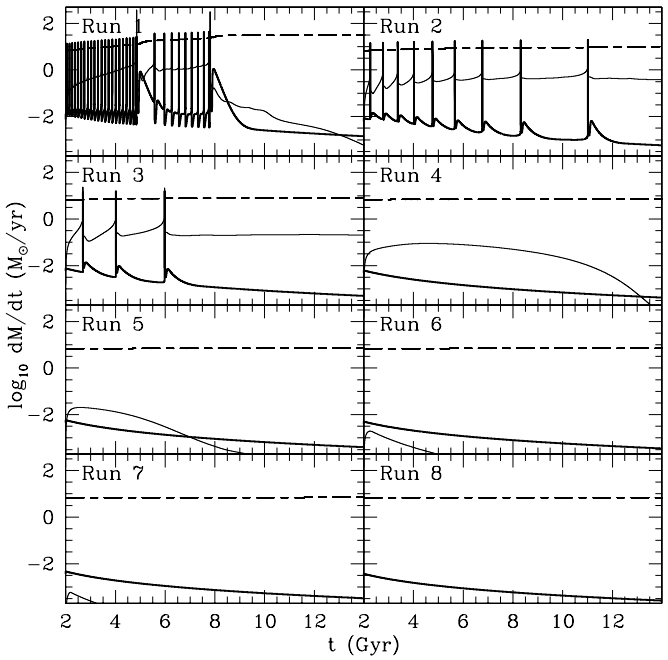

Figure 1. SMBH mass accretion rate $\dot{M}_{\rm BH}$ (thick line) and the SFR $\dot{M}_*$ (thin line) in the MA models. Both rates show a strong time dependence. The models with the lower feedback efficiency generally produce higher $\dot{M}_{\rm BH}$ and $\dot{M}_*$ more frequently. The Eddington accretion rate (short-long dashed line) is usually higher than $\dot{M}_{\rm BH}$ except for the peak activities.

For these reasons, we test eight different values of $\epsilon_{\rm w}^{\rm M}$ for both model MA and MB ranging from 1×10^{-5} to 5×10^{-2} (see Table 1). Because our goal is to constrain the range of acceptable efficiencies and models with the purely mechanical feedback, the tests also include unreasonably low and high values of $\epsilon_{\rm w}^{\rm M}$. We note that a model without AGN feedback effects was shown completely unreasonable in Paper I, producing an extremely massive SMBH.

3. RESULTS OF THE MA MODELS

As we explained in the previous section, the family of the MA models, i.e., the mechanical feedback models with a fixed feedback efficiency, has been widely adopted in various papers as the simplest prescription of AGN feedback. In Paper I, it is shown how these models are characterized by a quite rigid behavior with a sharp transition from very strong feedback effects to almost no effects, even though the input physics is quite elaborate. Here, we explore other aspects of these models, starting with the commonly used $\epsilon_{\rm w}^{\rm M} = 0.005$ (Run 6), and then progressively reducing it from Run 6 to Run 1 and increasing from Run 6 to Run 8.

3.1. Evolution of the MA Models

Figures 1 and 2 present the time evolution of some global quantities in the MA models. In all runs, the peak of the SFR ($\dot{M}_*$) is reached earlier than the peak of the SMBH mass accretion rate ($\dot{M}_{\rm BH}$); in some cases the two peaks are coincident within the limit of the simulation time resolution. High feedback efficiencies generally delay an initial starburst and a high $\dot{M}_{\rm BH}$,

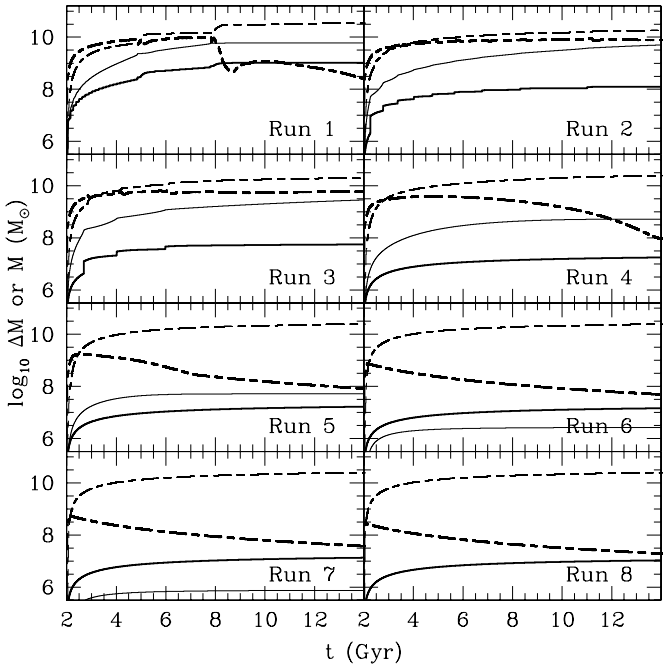

Figure 2. Time evolution of the mass budget in the MA models: the change of the SMBH mass $\Delta M_{\rm BH}$ (thick solid line), the change of the stellar mass ΔM_* (thin solid line), the total mass of gas within 10 $R_{\rm e}$ in the galaxy $M_{\rm g}$ (thick short-long dashed line), and the time-integrated mass of blown-out gas $\Delta M_{\rm w}$ (thin short-long dashed line). Following the difference in $\dot{M}_{\rm BH}$ and $\dot{M}_*$, models with different efficiencies result in different evolution of the mass ratio between the central SMBH and stars. $M_{\rm g}$ decreases because the total SMBH accretion rate, star formation rate, and galactic wind rate dominate at late times over the stellar mass-loss rate.

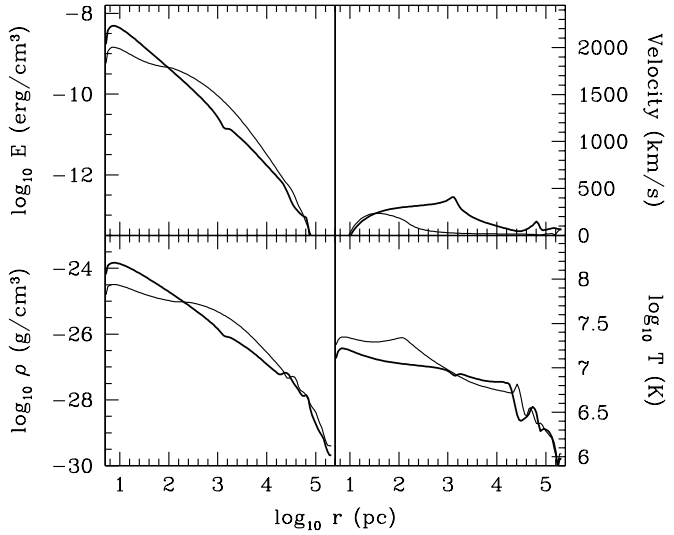

Figure 3. Radial structure of the gas internal energy density, velocity, mass density, and temperature in the MA model with $\epsilon_{\rm w}^{\rm M} = 5 \times 10^{-5}$ (Run 2), at $t =$ 3.5 Gyr (thick line) and 5.5 Gyr (thin line), corresponding to inter-burst phases (see Figure 1). The distributions of internal energy density and mass density do not change significantly between the two epochs.

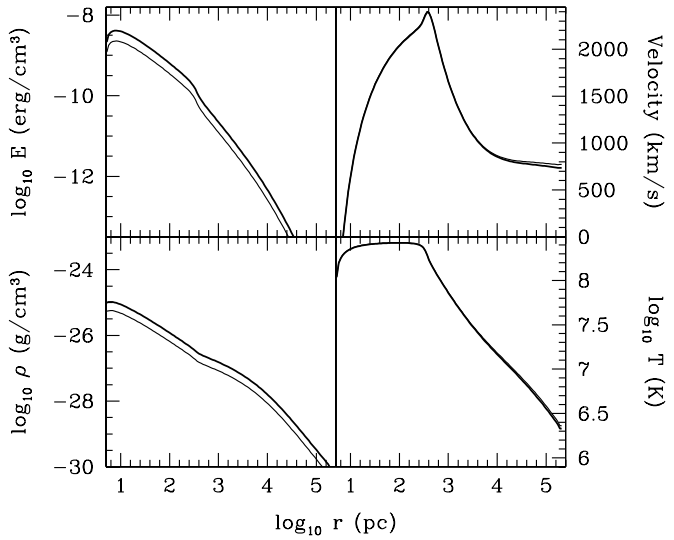

Figure 4. Radial structure of gas properties in the MA model with $\epsilon_{\rm w}^{\rm M} = 5\times10^{-3}$ (Run 6) at the same epochs as Figure 3. The comparison with Run 2 (Figure 3) shows that the velocity field and temperature distribution strongly depend on the feedback efficiencies. The high feedback efficiency induces the high-velocity outflow, the increase in gas temperature which is characterized by a flat high-temperature region of about 100 pc, and the corresponding low value of the central density. This trend is consistent with the overall suppression of both mass accretion to the SMBH and star formation, as seen in Figure 2.

and stop early further star formation and SMBH mass accretion. As found in the simulations from the Run 4 to 8 with high values of $\epsilon_{\rm w}^{\rm M}$, the effective time scale of the feedback process is so short that any peaked formation of stars and mass accretion to the central SMBH does not occur at all. Meanwhile, the low feedback efficiencies make galaxies have extended star formation and SMBH mass accretion with multiple peaks.

Remarkably, the main difference caused by different feedback efficiencies is discovered in the rise in stellar mass ΔM_* and SMBH mass $\Delta M_{\rm BH}$. If the initial ratio $M_{\rm BH}/M_*$ needs to be maintained at all times, $\Delta M_{\rm BH}/\Delta M_*$ is required to follow the same initial ratio $\sim 10^{-3}$. Yet, ΔM_* is always higher than $\Delta M_{\rm BH}$ for $\epsilon_{\rm w}^{\rm M} = 5\times10^{-4}$, while this trend is reversed for high feedback efficiencies, as shown in Figure 2. Therefore, our simulations imply extreme fine tuning of the efficiency $\epsilon_{\rm w}^{\rm M}$ in order to maintain the SMBH-to-stellar mass ratio at a constant level.

Different feedback efficiencies also affect the radial structure of gas. As shown in Figures 3 and 4, models with the high feedback efficiency are more likely to produce a high-velocity outflow at a large distance. For example, at $r \sim 20$ kpc, the outflow velocity is about 800 km s^{-1} for Run 6 ($\epsilon_{\rm w}^{\rm M} = 5\times10^{-3}$). But around the peak time of the SMBH mass accretion, the outflow in Run 2 ($\epsilon_{\rm w}^{\rm M} = 5\times10^{-5}$) has much lower velocity than 500 km s^{-1} at the same distance. High feedback efficiencies enhance the outflow as pointed out by Scannapieco & Oh (2004) and Levine & Gnedin (2005), even though SFR in their cases is not as high as in our simulation (David et al. 2006).

Heating by stellar processes and the additional AGN heating alters the temperature distribution of the gas within galaxies. As already discussed in numerous previous research (e.g., Tabor & Binney 1993; Binney & Tabor 1995; Ciotti & Ostriker 1997, 2001; Cattaneo et al. 2007), energy deposited by mechanical feedback heats up the surrounding ISM, resulting in a core structure of hot gas such as seen in Figures 3 and 4. Although the high feedback efficiency suppresses further star formation and stellar feedback processes, even in these cases the energy and mass supply by the strong AGN wind compensates for the lack of stellar feedback processes and finally heats up the gas.

As shown in Figure 5, the time evolution of the accretion luminosity is strongly coupled to the SMBH mass accretion history. However, we note that the luminosity at $t \sim 14$ Gyr is similar even for different values of feedback efficiencies, because the difference in the SMBH mass accretion rate is small at late times despite the difference of $\epsilon_{\rm w}^{\rm M}$. $L_{\rm BH}$ is generally lower than the Eddington luminosity for both high and low feedback

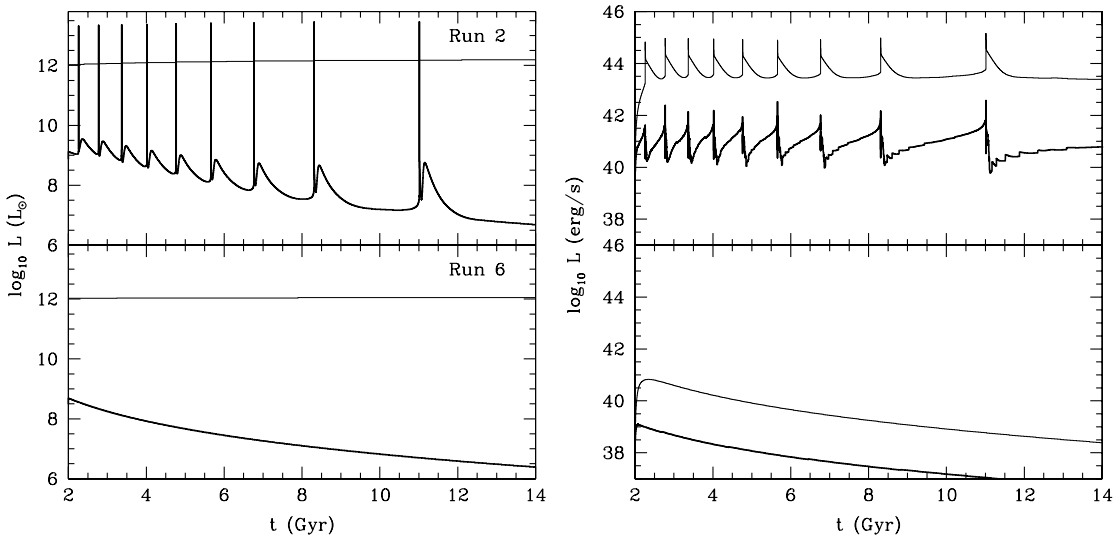

Figure 5. Time evolution of the dust-extincted optical accretion luminosity $L_{\rm opt}$ (left panel) and the X-ray luminosity from hot ISM within 10 $R_{\rm e}$ and infrared re-emission of stellar radiation (right panel) for Run 2 and 6. $L_{\rm opt}$ (thick solid line) is basically coupled to the mass accretion history shown in Figure 1, but it is usually much lower than the 10% of the Eddington luminosity (thin solid line). Only models with low feedback efficiencies achieve the optical luminosity which is higher than the 10% of the Eddington luminosity for short periods. The overall change of the X-ray luminosity from hot gas (thick line) and the infrared re-radiation of stellar light by dust (thin line) follows the evolution of SFR rather than the history of the SMBH mass accretion. But right after the peaks of the SMBH accretion rate in Run 2, the X-ray luminosity (thick line) declines more quickly than the infrared emission. This difference implies that the X-ray luminosity may be a more sensitive probe to measure the effects of AGN feedback on the ISM than IR emission.

efficiencies. Bursts of high $L_{\rm BH}$ above the Eddington luminosity are found only in the models with low feedback efficiencies such as Run 2. As we explain in the Appendix, our AGN model permits a moderate super-Eddington accretion. The AGN feedback with the low efficiency is not strong enough to stop the development of cold gas when the precursor of a large amount of cold gas reaches the central region. Therefore, a large fraction of the cold gas is accreted to the central SMBH at the end.

We find that the star formation history is mainly parallel to the evolution of both the X-ray luminosity from the hot diffuse ISM and the infrared (IR) emission by dust, which re-radiates the absorbed stellar radiation, as shown in Figure 5. As the difference in the star formation history implies in Figure 1, the difference in X-ray and IR luminosity is more significant for different feedback efficiencies than the difference in $L_{\rm BH}$. In addition, the X-ray luminosity of hot ISM intricately changes more than the IR emission, corresponding to the energy input from the AGN feedback and the mass loss by the continuously escaping hot gas (see Figure 2).

3.2. Are the MA Models Acceptable?

Figure 6 summarizes the results of our tests on the MA models. The mass ratio between the central SMBH and the host galaxy at 14 Gyr, i.e., $z \sim 0$, monotonically increases as the feedback efficiency decreases. For $\epsilon_{\rm w}^{\rm M} > 1 \times 10^{-4}$, the growth of stellar and SMBH mass is so small that the deviation from the initial ratio is not significant. Following the increased SMBH accretion, the net lifetime of bright AGN phase is also long in the models with the low $\epsilon_{\rm w}^{\rm M}$. When we adopt the B-band magnitude $M_{\rm B} < -23$ mag as a limit of optical quasars (Martini 2004) and use the typical spectral energy distribution of quasars (Elvis et al. 1994), the observational constraint on the maximal net lifetime is about 1 Gyr (Martini 2004). Even though there is no well-defined observational limit on the net lifetime when the bolometric luminosity $L_{\rm BH}$ is higher than 10% of the Eddington luminosity $L_{\rm Edd}$, Hopkins et al. (2005) claim that it is comparable to the lifetime of the optical limit on quasars. We find that the two measurements can be comparable for only $\epsilon_{\rm w}^{\rm M} \gg 10^{-5}$. But if our models have to reproduce any quasar phases since 2 Gyr, $\epsilon_{\rm w}^{\rm M} \gg 10^{-4}$ is not acceptable because it does not permit any strong SMBH accretion phases as shown in Figure 1 and does not experience any luminous phases with $M_{\rm B} < -23$ mag or $L_{\rm BH} > 0.1 L_{\rm Edd}$.

The episodic quasar lifetime can be used to constrain our models in addition to the net quasar lifetime. The episodic lifetime is measured for each instance of the quasar phase, i.e., the high SMBH accretion phase, while the net lifetime is the sum of the episodic lifetime for all instances. Because our models do not provide any information about quasar activity before the initial time of simulations, i.e., 2 Gyr, the net quasar lifetime of the models can be increased up to 2 Gyr further. Therefore, the episodic quasar lifetime can be a better diagnostic in our simulations. In Figure 7, we present the change of the episodic lifetime for $L_{\rm BH} > L_{\rm Edd}$ as an example. This episodic lifetime does not change significantly for every episodic activity, having a typical duration 0.4 Myr which is longer than both a fixed simulation output time-step size 0.1 Myr and varying computational time-step sizes (in average, about 50 yr). The episodic lifetime for $M_{\rm B} < -23$ mag also has the same pattern, but is about 1 Myr which is acceptable compared to a recent measurement (Kirkman & Tytler 2008).

We also compare the predicted X-ray luminosity of the hot ISM and the mass fraction of recently formed stars to the available observational constraints. The constraint on the X-ray luminosity is derived from the typical X-ray luminosity of local ellipticals (O'Sullivan et al. 2001) after subtracting the contribution of discrete X-ray sources from the X-ray luminosity (Ciotti et al. 1991; Kim & Fabbiano 2004). As shown in Figure 6, if the feedback efficiency is too low as in the model with $\epsilon_{\rm w}^{\rm M} = 1 \times 10^{-5}$, too much mass is accreted to the central SMBH, decreasing the X-ray luminosity and suppressing the late star formation. Meanwhile, the low SFR in the models with high feedback efficiencies causes the lack of hot gas, which sequentially results in low X-ray luminosities. Although the temperature of the hot gas is higher in models with the high feedback efficiencies, the total amount of gas is too low to be

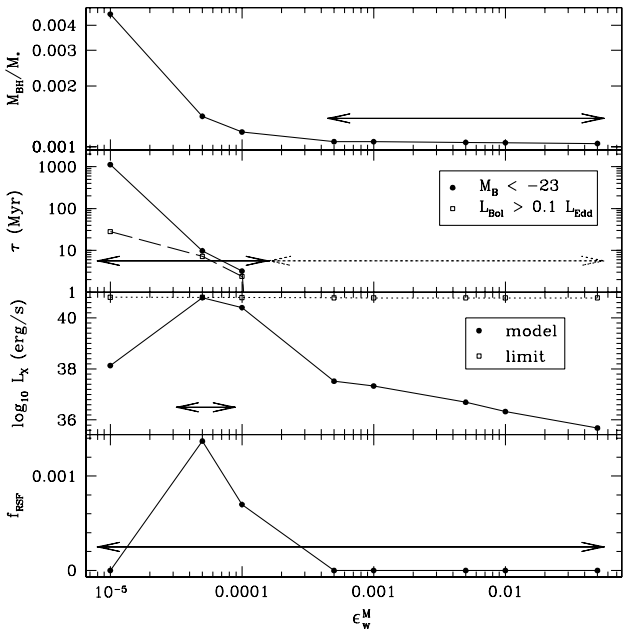

Figure 6. Results of the four proposed tests for the MA models at the epoch of 14 Gyr. From top to bottom, four tests are the SMBH mass to stellar mass ratio, the net quasar lifetime, the X-ray luminosity of the diffuse hot gas inner 10 R_e, and the fraction of stellar mass formed within the last 1 Gyr f_{RSF}. The ratio M_{BH}/M_* in simulations can be consistent with observations for $\epsilon_w^M > 1\times10^{-4}$. Yet, L_X is inconsistent for $\epsilon_w^M > 1\times10^{-4}$, and the corresponding models do not experience quasar-like phases. The arrow bars represent the range of ϵ_w^M that is acceptable for each test. For the net quasar lifetime, $\epsilon_w^M \gg 10^{-4}$, which is represented by the dotted arrow bar, is acceptable only if our models do not need to experience any quasar phases in the evolution.

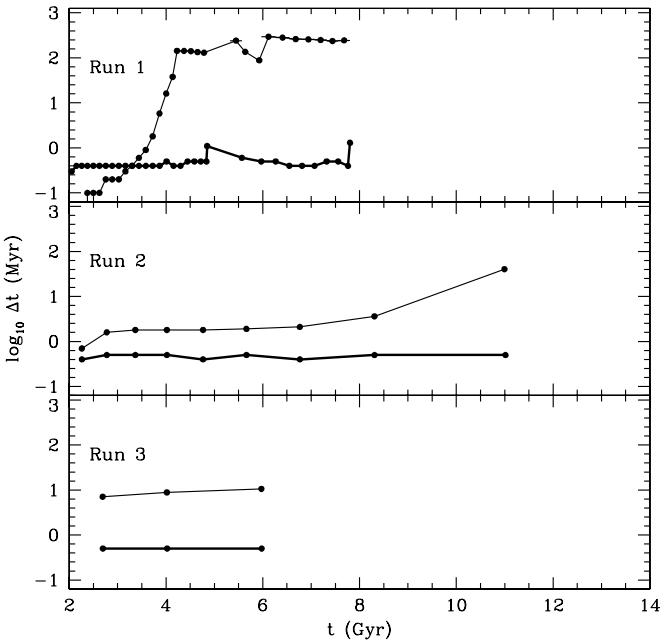

Figure 7. Episodic lifetime of intensive star formation and quasar activity in the MA models. For Run 1–3, we measure the episodic lifetime of SFR $M_\odot > 1\ M_\odot\ \mathrm{yr}^{-1}$ (thin line) and when the bolometric luminosity from the central SMBH L_{BH} is higher than the Eddington luminosity L_{Edd} (thick line). The typical episodic lifetime of $L_{BH} > L_{Edd}$ is about 0.4 Myr for all three simulations at any time. The high SFR generally shows a long duration at late time.

compensated by the high temperature. However, it is important to recall that all models explored in this paper represent a galaxy that is initially devoid of gas and without external pressure (see Pellegrini et al. 2009). The measured recently formed stellar mass for the last Gyr is lower than a few percent in local elliptical galaxies (Yi et al. 2007; Donas et al. 2007; Kaviraj et al. 2007), which is much higher than what we find in our MA models. Hence, the fraction of recently formed stellar mass in simulation results is acceptable compared to local ellipticals.

The duration of SFR $M_* > 1\,M_\odot\,\mathrm{yr}^{-1}$ depends on when intensive star formation occurs and how strong the feedback efficiency is. Generally, the late star formation has a longer duration. For example, the late star formation in Run 1 continues longer than 100 Myr, as shown in Figure 7. The effect of different feedback efficiencies is significant in modulating the early star formation. For example, in Run 3 the peaked early star formation lasts for about 10 Myr. Yet, the low feedback efficiency in Run 1 allows the accretion to the central SMBH to occur more frequently, resulting in the short duration of vigorous star formation.

In short, it is difficult to find the range of the feedback efficiency in the MA model that satisfies the four observational constraints together. Low efficiencies ($\epsilon_w^M < 5\times10^{-4}$) produce too massive central SMBHs or long net lifetime of quasar activity. High efficiencies ($\epsilon_w^M > 5\times10^{-5}$) have different problems: too low X-ray luminosity or no quasar activity. Importantly, the popularly used $\epsilon_w^M = 0.005$ does not pass the four tests simultaneously.

4. RESULTS OF THE MB MODELS

We now move to discuss the MB models. In these models, the mechanical output from the central SMBH depends on the accretion luminosity, increasing as a function of L_{BH}/L_{Edd} as presented in Equation (3). This description is definitely more close to the real processes around the central SMBHs than the fixed mechanical feedback efficiency in the MA models (Kurosawa & Proga 2009). As we will see, however, the basic consequence of varying the feedback efficiency is qualitatively same in MA and MB models, despite their differences.

4.1. Evolution of the MB Models

The peak value of the feedback efficiency ϵ_w^M determines how frequently the SMBH and its host galaxy can achieve high SMBH mass accretion rate and SFR, as we already found in the MA models. Figure 8 presents the SMBH mass accretion rate and SFR in the MB models. Either extremely high or low feedback efficiencies does not permit the resurrection of both high $\dot{M}_{BH}$ and $\dot{M}_*$. For example, in Run 1 SFR is higher than the SMBH mass accretion rate at any time, while the reversed pattern of growth rates is found in Run 8.

The peak feedback efficiency also determines the onset of the earliest burst and the last burst in $\dot{M}_{BH}$ and $\dot{M}_*$. In Run 1 with $\epsilon_w^M = 1\times10^{-5}$, the initial effect of mechanical feedback is too weak to suppress the growth of the SMBH mass, even though star formation is always calm. As seen from Run 2 to 7 in Figure 8, increasing ϵ_w^M prevents the early intensive mass accretion onto the BH, but the global SFR is not initially affected by the high feedback efficiencies. High feedback efficiencies also cause the early cessation of repeating peaked high $\dot{M}_{BH}$ and $\dot{M}_*$. For example, the last peak $\dot{M}_{BH}$ of Run 7 is found to be about 5 Gyr earlier than that of Run 5.

The change of the total mass in each run is summarized in Figure 9. We do not find a strong variability in the mass of the ejected gas and gas inside a galaxy despite the large difference in feedback efficiencies, while we found a significant difference among the MA models. The main difference is found in the total mass of stars and the central SMBH, following the difference

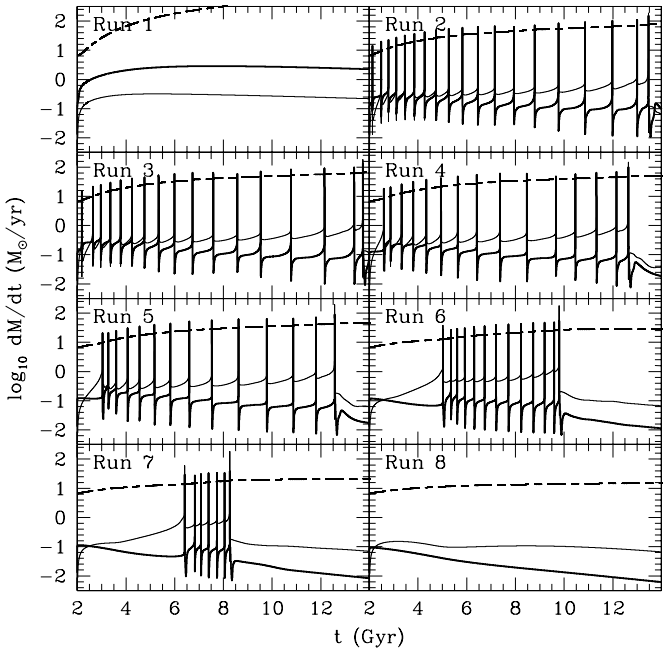

Figure 8. SMBH mass accretion rate $\dot{M}_{\rm BH}$ (thick line) and SFR $\dot{M}_*$ (thin line) in the MB models. The Eddington accretion rate (short-long dashed line) is always much higher than $\dot{M}_{\rm BH}$ except for the peak activities, as found in the MA models. In the models with either extremely high or low feedback efficiencies, self-regulated outbursts are not found, showing almost constant or decreasing $\dot{M}_{\rm BH}$ and $\dot{M}_*$. Compared with the MA models, the MB models substantially increase the number of bursts because $\epsilon_{\rm w}$ is low at low accretion luminosity, and this favors a quick accumulation of recycled gas in the galaxy.

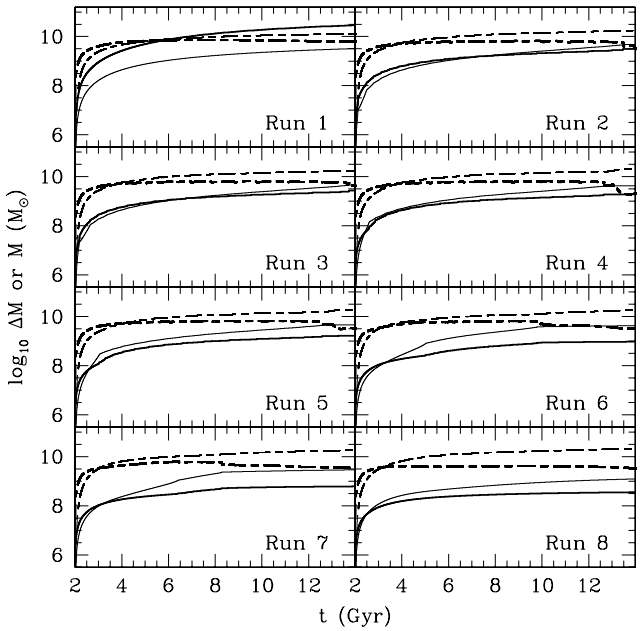

Figure 9. Time evolution of the mass budget in the MB models: the change of the SMBH mass $\Delta M_{\rm BH}$ (thick solid line), the change of the stellar mass ΔM_* (thin solid line), the total mass of gas within 10 $R_{\rm e}$ in the galaxy $M_{\rm g}$ (thick short-long dashed line), and the time-integrated mass of blown-out gas $\Delta M_{\rm w}$ (thin short-long dashed line). Only $\Delta M_{\rm BH}$ depends strongly on the feedback efficiency. Because SFR is generally higher than $\dot{M}_{\rm BH}$ as shown in Figure 8, the increase in stellar mass outpaces that of the SMBH mass during the early evolution.

in the evolution of $\dot{M}_{\rm BH}$ and $\dot{M}_*$ in Figure 8. In all simulations except for Run 1, the increase in stellar mass overwhelms the growth of the central SMBH before approximately 8 Gyr. As we find in the MA models, the MB model also shows that the dynamically evolving model of AGN feedback naturally results in the time-dependent mass ratio between the central SMBH and its host galaxy.

The importance of physics-based feedback models is obviously found by comparing Figures 2 and 9. Even for the same radiation conversion efficiency from the accretion mass, the MA model is more effective than the MB model in supplying feedback energy and suppressing the growth of both stellar and SMBH mass. Although the maximum instantaneous feedback effect is same for the same $\epsilon_{\rm w}^{\rm M}$ in both models, the higher feedback effect in the MA models at low accretion rates leads to quite important differences. This difference finally affects how frequently intensive AGN activity and star formation is restored.

The impact from the differences between MA and MB models is particularly apparent for very low feedback efficiencies. For Run 1 with $\epsilon_{\rm w}^{\rm M} = 1 \times 10^{-5}$, the SMBH accretion rate is almost constant at the high value of $10^{0.4}\,M_\odot\,{\rm yr}^{-1}$ in the MB model, while the rate strongly fluctuates up to about 8 Gyr in the MA model. The luminosity dependence of $\epsilon_{\rm w}$ in the MB models allows more rapid growth of the central SMBH than in the MA models. And then the very large value of $L_{\rm Edd}$ with the large $M_{\rm BH}$ consequently reduces $\epsilon_{\rm w}$ following Equation (3) in the MB models. Therefore, the evolution quickly turns into a runaway state, while the central SMBH grows. Even though either very low or high values of $\epsilon_{\rm w}^{\rm M}$ does not show bursting activity (see Figure 8), in Run 1 $M_{\rm BH}$ is much higher than that in Run 8 because the runaway process prevents bursts with increasing $M_{\rm BH}$ in Run 1, but simply high feedback efficiency in Run 8 prevents both the bursts of $\dot{M}_{\rm BH}$ and the increase in $M_{\rm BH}$.

4.2. Problems of the MB Models

As we find in the tests with the MA models, the family of the MB models also appears to fail to pass our tests. Low feedback efficiencies produce too massive central SMBHs and too long net lifetime of quasar activity as presented in Figure 10, while the ratio $M_{\rm BH}/M_*$ is much higher than the locally found value of about 10^{-3}. Moreover, the net lifetime of quasar phase at $M_{\rm B} < -23$ mag is not matched to the limit of 1 Gyr (Martini 2004). As found in the MA model, the recently formed stellar mass in the MB models is also much lower than the observational maximum limit. However, the thermal X-ray luminosity for any value of $\epsilon_{\rm w}^{\rm M}$ except for Run 1, does not conform to the observational limits.

The episodic lifetime of quasar activity and significant star formation does not have a systematic difference in the MB models compared to the MA models. The duration of the last burst is considerably longer than those at earlier times as shown in Figure 11. The first starburst is also longer than other peaks of SFR in the models with low feedback efficiencies such as Run 7. The duration of the bright quasar phase weakly changes considering the limit of $L_{\rm Bol} > L_{\rm Edd}$. But we note that the duration of episodic activity is subject to how we define the limit of activity.

The family of the MB models also fails to conform to four major observational constraints considered together. The fraction of recently formed stellar mass does not play a key role as an important diagnosis because of its poor sensitivity to variation of the feedback efficiency. The net lifetime of quasar phase is strongly coupled to the change of the SMBH mass accretion, as we find in the MA models. The X-ray luminosity of hot ISM turns out to be a useful diagnosis to test the feedback physics again in the MB models. The X-ray luminosity favors $\epsilon_{\rm w}^{\rm M} < 5 \times 10^{-5}$. But this range is much lower than $\epsilon_{\rm w}^{\rm M} > 10^{-2}$

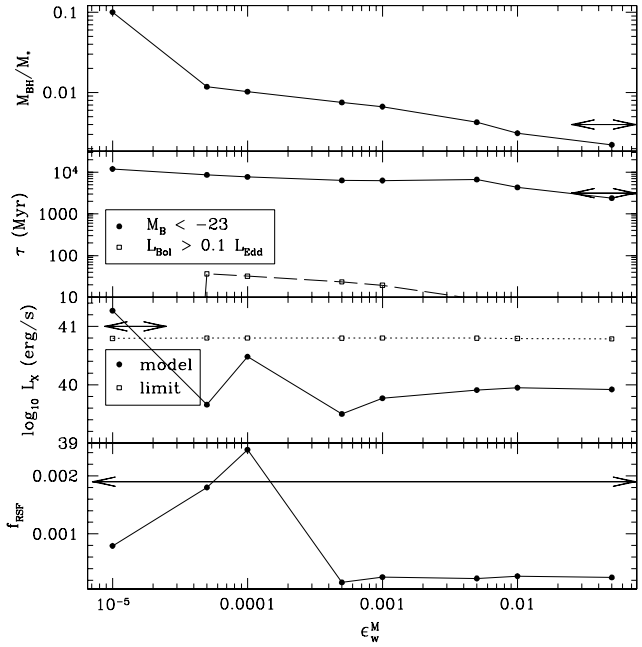

Figure 10. Results of the four tests for the MB models at the epoch of 14 Gyr. From top to bottom, simulation results are compared to four observational constraints: the SMBH mass to stellar mass ratio, the net quasar lifetime, the X-ray luminosity of diffuse hot gas, and the fraction of stellar mass formed within the last 1 Gyr. The low ϵ_w^M in the MB models enhances the growth of the central SMBH, resulting in the high values of M_{BH}/M_* and net quasar lifetime. The arrow bars represent the range of ϵ_w^M that is consistent with observations. This comparison shows that none of the tested feedback efficiencies can pass all tests simultaneously.

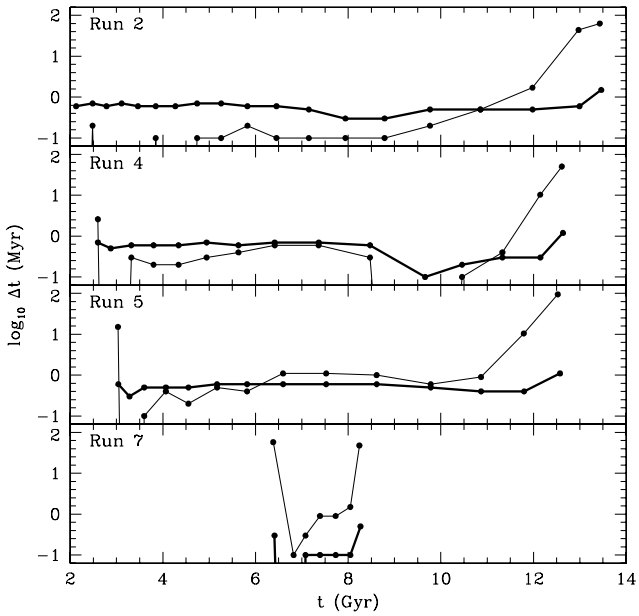

Figure 11. Episodic lifetime of intensive star formation and quasar activity in the MB models. For the same limits of SFR and the bolometric luminosity from the central SMBH used in Figure 7, the MB model also shows the same pattern as the MA model shows. Late bursts of star formation (thin line) are maintained longer than early bursts. The duration of $L_{BH} > L_{Edd}$ (thick line) is between 0.1 Myr and 1 Myr generally without a significant dependence on ϵ_w^M.

which produces the right ratio between the SMBH and its host galaxy mass.

5. OTHER POSSIBLE DIAGNOSTICS

In addition to four tests adopted in this paper, we find additional possible diagnostics which have not been well investigated observationally, but which can be valuable to constrain various AGN feedback models. In particular, the feedback efficiencies need to be refined more precisely even in the purely mechanical feedback models because of the possibility that the feedback efficiency may be dependent of the SMBH mass and other properties (e.g., Merloni & Heinz 2008). Therefore, finding an effective tool of diagnosis is quite important.

The current ratio of the SMBH accretion rate to the SMBH mass can be a constraint on the feedback efficiencies for different feedback models. As shown in Figures 1, 8, and 12, the cumulative effects of the self-regulation process result in the difference in the SMBH mass and the current accretion rate (see Netzer & Trakhtenbrot 2007, for a discussion). This ratio $\dot{M}_{BH}/M_{BH}$ can be converted to the observable quantity L_{BH}/L_{Edd} which are lower than 10^{-3} in local low-luminosity AGNs and 0.1–1 in classical luminous local AGNs (Ho 2008). As we find in Figures 7 and 11, this ratio changes quickly within 1 Myr even though the duration of $L_{BH}/L_{Edd} > 1$ is quite insensitive to the feedback models and their efficiencies. The main concern in observation is measuring the statistical distribution of this ratio for broad ranges of AGN activity levels as well as a quite phase (Kim et al. 2008).

The central density and temperature of hot ISM is also an interesting quantity of the feedback model (e.g., Pellegrini et al. 2009). The simulations show that the total amount of gas and its temperature change responding to the energy input by different AGN feedback models. In addition to this global change, the change of hot ISM in the central region around the SMBH shown in Figure 13 can be compared to observations for the same range of the central SMBH and host galaxy mass. For example, the observed central density of electrons in a few local quiescent ellipticals is about 0.02 cm^{-3} which corresponds to the mass density $\rho \sim 10^{-26}$ g cm^{-3} (Humphrey et al. 2006; Soria et al. 2006a, 2006b), which is not very different from the values presented in Figure 13. But as the observational values also depend on the specific galaxy models adopted, proper comparisons can be obtained by focusing on a well-observed galaxy for which the dynamical and structural properties are well constrained by independent studies, or by studying statistically a large set of observed profiles of density and temperature for the X-ray emitting gas. Because we do not include recent accretion of external gas or major/minor galaxy mergers, a direct comparison of our simulations results to observations need to be limited to local ellipticals not showing dynamical and structural properties of recent accretion or mergers. Moreover, the best comparison between our simulations and observations is possible only with the simultaneous measurements of the SMBH mass and its accretion rate too.

6. DISCUSSION AND CONCLUSION

We have shown that the implementations of two simple classes of purely mechanical feedback models are not likely to satisfy the four major observational constraints when considered together. Importantly, there does not seem to be any possible range of the mechanical feedback efficiencies, including the commonly used $\epsilon_w^M = 0.005$, which can be compatible with the observations, The simulation results also prove that the self-regulation process by AGNs requires a careful consideration of both the timing problem and of the energy conversion problem. As we will discuss in a subsequent paper, the models including both mechanical and radiative feedback may be a right approach

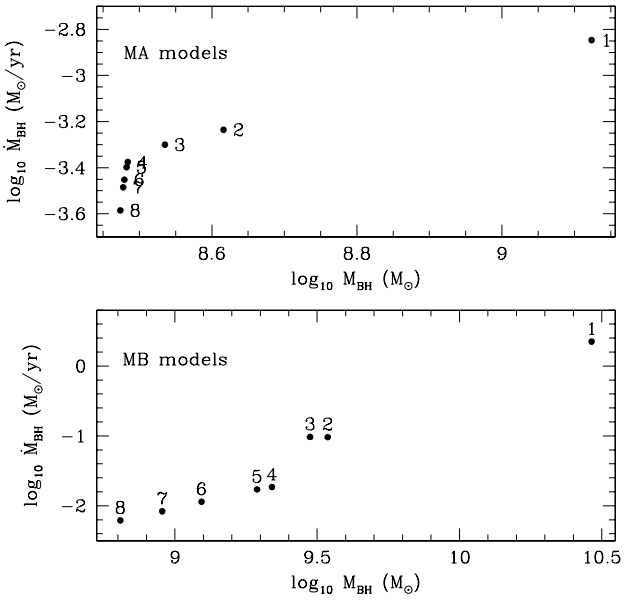

Figure 12. Distribution of the SMBH accretion rate vs. its mass at 14 Gyr for all models in Table 1. The numbers near the points are the names of the simulation runs. The difference between MA and MB models results is apparent in the different ranges of $M_{\rm BH}$ for the same initial SMBH mass. In both models, high accretion rates correspond to low feedback efficiencies. But we note that the central SMBHs in all models are not in an active phase at 14 Gyr as shown in Figures 1 and 8.

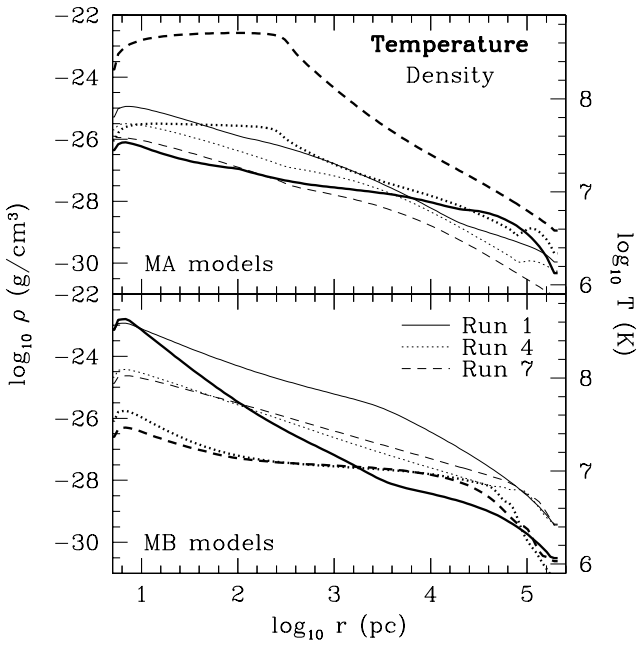

Figure 13. Radial temperature and density distribution of hot gas in Run 1, 4, and 7 at 14 Gyr when the SMBH accretion rate is much lower than the Eddington accretion rate. In both MA and MB models, the high feedback efficiencies result in the low central density (thin line). However, the temperature profile (thick line) is dependent of which feedback prescription is used. In particular, the temperature core in the MA models is produced by the constant feedback efficiency, while in MB models the low accretion luminosity at 14 Gyr produces a very weak feedback which makes the temperature profile be similar to a standard low-luminosity hot accretion profile.

to simulate the self-regulation process as we observe in local luminous quasars.

The simulations presented in this paper do not consider departures from spherical symmetry, nor chemical evolution of stellar and gas metallicity in addition to other shortcomings such as the effects of external gas pressure and accretion of stars to SMBH (e.g., Jogee 2006; Pellegrini et al. 2009). Because of these missing parts with the present approach, it is not possible to exploit other well-derived observational constraints on the feedback models. For instance, the commonly observed extended emission line regions around quasars are mainly understood as the consequence of geometrically complex outflows driven by either radiative or mechanical wind during the intensive AGN phase (Batcheldor et al. 2007; Letawe et al. 2008; Fu & Stockton 2009). Testing simulations based on the properties of the outflows will require one to resolve three-dimensional spatial structure, as various hydrodynamic or radiative instabilities are not caught in one-dimensional simulations. We note, however, that the adopted prescriptions for the mechanical AGN feedback effects are based on sub-grid physics corresponding to mass, momentum, and energy transportation in small-scale turbulent motions, even though the simulations assume a spherical symmetry. Implementing chemical evolution models in our simulations would be a necessary step to use the observed metallicity gradients and average metallicities of elliptical galaxies as another diagnostic (e.g., Carollo et al. 1993; Gibson 1996). Even though the effects from AGN feedback on galactic metallicity gradients have not been carefully considered in the current observational investigations (Sánchez-Blázquez et al. 2007), this assumption needs to be verified in the AGN feedback models with chemical evolution by comparing simulation results with observed gradients (Matteucci & Padovani 1993; Friaca & Terlevich 1998; Angeletti & Giannone 2003; Ballero et al. 2008; Kisaka et al. 2008; Spolaor et al. 2009).

In our simulations, we do not consider the problem of the common evolution of the SMBH mass and of the stellar mass during the initial phases of galaxy formation. The simulations begin with a galaxy already formed and a central SMBH. In particular, here we assume that the initial SMBH may have formed with the right mass ratio for the initial bulge (e.g., Elmegreen et al. 2008). But the establishment of the SMBH-to-stellar mass ratio, as well as the Faber–Jackson and the fundamental plane in the early evolution of ellipticals, is still poorly understood both observationally and theoretically (see Ciotti 2009 for a review). It will be interesting to test different initial central black hole to stellar mass ratios in future simulations. Because stellar mass determines the total amount of recycled gas, and AGN feedback models depend on SMBH mass, probably, different initial mass ratios and masses might result in complicated evolution which need to be carefully tested in simulations.

Minor mergers and cosmological gas accretion might not affect our main conclusions. As we explained in Section 1, major galaxy mergers might not be a significant effect on late galaxy evolution. But late minor mergers and accretion can play an important role in fueling gas onto SMBHs. Even in these cases, our main conclusions might not be strongly changed except for the test with the net lifetime of the luminous quasar phase. The net lifetime of the quasar phase depends on how many times strong gas fueling occurs, while other tests such as the simultaneous growth of SMBH and stellar mass and the episodic lifetime of the quasar phase is dominated by a feedback physics. Cosmological simulations including detailed AGN feedback effects such as our models will be a direct test of effects from minor mergers and gas accretion.

Despite their intrinsic limitations, our simulations bridge the gap between simple prescriptions of AGN feedback in cosmological studies or simulations of galaxy mergers, and examination of the small-scale physics around the central SMBHs.

The problem of the self-regulation process itself demands elaborate prescriptions of dynamical evolution and energy conversion around the central SMBH and its surrounding ISM. In this paper, we found additional evidence that purely mechanical feedback models, including some improved versions based on physical arguments, fail to pass basic observational constraints. Our next paper will present how combining both radiative and mechanical AGN feedback effects can produce the evolutionary models of elliptical galaxies that are more consistent with the properties of the central SMBHs and their host galaxies in local universe.

We are grateful to Michael Strauss, James Gunn, Gillian Knapp, Renyue Cen, and Christy Tremonti for useful discussions and careful reading. We thank the anonymous referee for considered comments which improved this manuscript. M.-S. is supported by the Charlotte Elizabeth Procter Fellowship of Princeton University. Computations were performed on the computational facilities of PICSciE (Princeton Institute for Computational Science and Engineering).

APPENDIX

A. INPUT PHYSICS

In this appendix, we summarize the implementation of the physics involved in the simulations. For a more extensive discussion the reader is referred to Ciotti & Ostriker (2007) and to Paper I.

A.1. The Hydrodynamical Equations

The evolution of the galactic gas flow is obtained integrating the time-dependent Eulerian equations of hydrodynamics:

$$\frac{\partial \rho}{\partial t} + \nabla \cdot (\rho v) = \alpha \rho_* + \dot{\rho}_{\rm II} - \dot{\rho_*}^+, \tag{A1}$$

$$\frac{\partial m}{\partial t} + \nabla \cdot (m v) = -(\gamma - 1)\nabla E - \nabla p_{\rm rad} + g\rho - \dot{m}_*^+, \tag{A2}$$

$$\frac{\partial E}{\partial t} + \nabla \cdot (E v) = -(\gamma - 1) E \nabla \cdot v + H - C + \frac{(\alpha \rho_* + \dot{\rho}_{\rm II})(v^2 + 3\sigma_*^2)}{2} + \dot{E}_{\rm I} + \dot{E}_{\rm II} - \dot{E}_*^+. \tag{A3}$$

ρ, m, and E are the gas mass, momentum, and internal energy per unit volume, respectively, and v is the gas velocity. The ratio of the specific heats is $\gamma = 5/3$, and $g(r)$ is the gravitational field of the galaxy (stars and dark matter), plus the contribution of the central SMBH. The gravitational field is updated at each time step by considering the SMBH mass growth; for simplicity, we do not take into account neither the ISM contribution, nor the mass redistribution due to the stellar mass losses and star formation. The total radiative pressure gradient is $\nabla p_{\rm rad} = (\nabla p_{\rm rad})_{\rm es} + (\nabla p_{\rm rad})_{\rm dust} + (\nabla p_{\rm rad})_{\rm photo}$, while $H-C$ is the radiative heating and cooling term.

The energy source term is obtained under the assumption that the streaming velocity of the source distribution is zero, neglecting the small contributions of the internal energy of the injected gas, and of the kinetic energy of stellar wind when compared to the local stellar velocity dispersion contribution (for the derivation and detailed discussion of the hydrodynamical equations with moving isotropic or anisotropic source terms, see D'Ercole et al. 2000). The source terms $\alpha\rho_*$ and $\dot{E}_{\rm I}$ of the initial, passively evolving stellar population, and the source terms due to Type II SNe, $\dot{\rho}_{\rm II}$ and $\dot{E}_{\rm II}$, are described in the following.

The first active grid point R_1 is placed within the Compton radius

$$R_{\rm X} = \frac{2GM_{\rm BH}\mu m_{\rm p}}{3k_{\rm B}T_{\rm X}} \simeq 3.6\mu \frac{M_{\rm BH}}{10^8\,M_\odot}\frac{10^7{\rm K}}{T_{\rm X}} \quad {\rm pc}, \tag{A4}$$

so that at R_1 we can impose the physical condition of a vanishing thermodynamical pressure gradient, leading to gas free fall on the circumnuclear disk when the radiation pressure is negligible; in this paper, we adopt $T_{\rm X} = 2.5\times10^7$ K. The appropriate values for radiation pressure at R_1 are obtained from the disk treatment.

The simulations are realized with a spatially second-order Eulerian scheme which adopts two staggered grids, each of them consisting of 120 logarithmically spaced grid points. The equations are integrated with a time-splitting scheme, while the heating and cooling terms in the energy equation are integrated by using a predictor-corrector scheme, so that the integration is second order in time. At each simulation time, the time step is determined as a fraction of the minimum among the Courant condition over the grid, and of the others characteristic times associated with the described physical processes: during the accretion phases (and subsequent bursts of radiation), it is not infrequent to have time steps of the order of one year or less. However, it is important to note the accretion events are characterized by the intrinsic time scale related to Equation (A4) by

$$t_{\rm X} \equiv \frac{R_{\rm X}}{c_{\rm X}} \simeq 1.22\,10^4\mu^{3/2}\frac{M_{\rm BH}}{10^8\,M_\odot}\left(\frac{10^7{\rm K}}{T_{\rm X}}\right)^{3/2} \quad {\rm yr}, \tag{A5}$$

where $c_{\rm X}$ is the isothermal sound velocity associated with the Compton temperature.

A.2. Stellar Passive Evolution: SNIa Rate and Stellar Mass Losses

The stellar mass-loss rate and the SNIa rate associated with the initial stellar distribution are the main ingredients driving evolution of the models. In the code the stellar mass losses—the source of fuel for the activity of the SMBH—follow the detailed prescriptions of the stellar evolution theory. Over the whole galaxy

$$\dot{M}_* = {\rm IMF}(M_{\rm TO})|\dot{M}_{\rm TO}|\Delta M, \tag{A6}$$

where the initial mass function (IMF) is a Salpeter law (normalized as described in CDPR), and the turn-off mass (in $M_\odot$) of stars at time t (in Gyr) is

$$\log M_{\rm TO} = 0.0558(\log t)^2 - 1.338\log t + 7.764. \tag{A7}$$

Finally,

$$\Delta M = \begin{cases} M_{\rm TO} - M_{\rm fin}(M_{\rm TO}) = 0.945 M_{\rm TO} - 0.503, \\ \quad (M_{\rm TO} < 9\,M_\odot), \\ M_{\rm TO} - 1.4\,M_\odot, \quad (M_{\rm TO} \geqslant 9\,M_\odot). \end{cases} \tag{A8}$$

The time evolution of the SNIa rate is parameterized as

$$R_{\rm SN}(t) = 0.32\times10^{-12}h^2\vartheta_{\rm SN}\frac{L_{\rm B}}{L_{\rm B\odot}}\left(\frac{t}{13.7\,{\rm Gyr}}\right)^{-s} \quad {\rm yr}^{-1}, \tag{A9}$$

where $h \equiv H_\circ/100$ km s^{-1} Mpc^{-1}, and the coefficient $\vartheta_{\rm SN}$ allow for different choices in the present-day SN Ia. Assuming for each SN event an energy release of $E_{\rm SN} = 10^{51}$ erg, a

fraction $\eta_{\rm SN}$ of which is thermalized in the surrounding ISM, the energy input per unit time over all the galaxy body is given by

$$L_{\rm SN}(t) = 1.015 \times 10^{31} h^2 \vartheta_{\rm SN} \eta_{\rm SN} \frac{L_{\rm B}}{L_{\rm B\odot}} \left(\frac{t}{13.7\,{\rm Gyr}}\right)^{-s} {\rm erg\,s^{-1}}; \quad \text{(A10)}$$

in this paper, we restrict to the case $\vartheta_{\rm SN} = 1$ and $h = 0.75$. Here, we restrict to the currently favored $s = 1.1$ value.

Besides energy, SNe provide also mass. We assume that each SNIa ejects $1.4\,M_\odot$ of material in the ISM, so that the total rate of mass return from the aging initial stellar population at each place in the galaxy is

$$\frac{d\rho_*}{dt} = (\alpha_* + \alpha_{\rm SN})\rho_*, \quad \text{(A11)}$$

where $\alpha_{\rm SN}(t) = 1.4\,M_\odot\,R_{\rm SN}(t)/M_*$ and $\alpha_*(t) = \dot{M}_*(t)/M_*$ are the specific mass return rates. With these definitions, the SNIa kinetic energy injection per unit volume in the ISM can be written as

$$\dot{E}_{\rm I} = \eta_{\rm SN} E_{\rm SN} \frac{R_{\rm SN}}{M_*}\rho_* = \eta_{\rm SN} E_{\rm SN} \frac{\alpha_{\rm SN}(t)\rho_*}{1.4\,M_\odot}. \quad \text{(A12)}$$

A3. Star Formation, SNII Heating, and Starburst Properties

Star formation cannot be avoided when cool gas accumulates in the central regions of elliptical galaxies. In particular, we compute the star formation rate at each radius r from the equation

$$\dot{\rho_*}^+ = \frac{\eta_{\rm form}\rho}{\tau_{\rm form}}, \quad \tau_{\rm form} = \max(\tau_{\rm cool}, \tau_{\rm dyn}), \quad \text{(A13)}$$

where ρ is the local gas density, $\eta_{\rm form} = 0.03 - 0.4$, and the associated characteristic times are

$$\tau_{\rm cool} \equiv \frac{E}{C}, \quad \tau_{\rm dyn} = \min(\tau_{\rm Jeans}, \tau_{\rm rot}),$$
$$\tau_{\rm Jeans} \equiv \sqrt{\frac{3}{32\pi G\rho}}, \quad \tau_{\rm rot} \equiv \frac{2\pi r}{v_c(r)}. \quad \text{(A14)}$$

E and C are the gas internal energy and the effective cooling per unit volume, while $v_c(r)$ is the galaxy rotational velocity at radius r. In the code, the stars are maintained in the place where they form, and in each shell the associated sinks of momentum and internal energy per unit volume are given by the negative of

$$\dot{m}_*^+ = \frac{\eta_{\rm form} m}{\tau_{\rm form}}, \quad \dot{E}_*^+ = \frac{\eta_{\rm form} E}{\tau_{\rm form}}, \quad \text{(A15)}$$

where m is the specific momentum of the ISM.

For a total mass ΔM_* of newly formed stars in a given time step and at a given place, we assume a Salpeter IMF

$$\frac{dN}{dM} = (x-1)\left(\frac{M_{\rm inf}}{M_\odot}\right)^{x-1}\frac{\Delta M_*}{M_\odot} \times \left(\frac{M}{M_\odot}\right)^{-1-x}, (x > 1, M \geqslant M_{\rm inf} = 0.1\,M_\odot), \quad \text{(A16)}$$

so that the associated total number of Type II SNe is

$$N_{\rm II} = \int_{M_{\rm II}=8\,M_\odot}^{\infty} \frac{dN}{dM} dM = \left(1 - \frac{1}{x}\right) \times \left(\frac{M_{\rm inf}}{M_{\rm II}}\right)^x \frac{M_\odot}{M_{\rm inf}} \frac{\Delta M_*}{M_\odot} \simeq 7 \times 10^{-3} \frac{\Delta M_*}{M_\odot}, \quad \text{(A17)}$$

where the numerical value holds for $x = 1.35$. As for SNIa, we assume that each SNII event releases $E_{\rm SN} = 10^{51}$ erg of kinetic energy, and the resulting mean efficiency is

$$\epsilon_{\rm II} \equiv \frac{N_{\rm II} E_{\rm SN} \eta_{\rm SN}}{\Delta M_* c^2} = \left(1 - \frac{1}{x}\right) \times \left(\frac{M_{\rm inf}}{M_{\rm II}}\right)^x \frac{M_\odot}{M_{\rm inf}} \frac{E_{\rm SN}\eta_{\rm SN}}{M_\odot c^2} \simeq 3.9 \times 10^{-6} \eta_{\rm SN}; \quad \text{(A18)}$$

in this paper, we assume $\eta_{\rm SN} = 0.85$. The characteristic time for SNII explosion is fixed to $\tau_{\rm II} = 2 \times 10^7$ yr, and from Equations (A13) and (A18) their luminosity (per unit volume) at each radius from the galaxy center is

$$\dot{E}_{\rm II}(t) \equiv \frac{\epsilon_{\rm II} c^2}{\tau_{\rm II}} \int_0^t \dot{\rho_*}^+(t') e^{-(t-t')/\tau_{\rm II}} dt'. \quad \text{(A19)}$$

We assume that each explosion leaves a neutron stars of $1.4\,M_\odot$. As a consequence, the total mass ejected by the SNII explosions per unit mass is

$$\frac{M_{\rm II}^{\rm ej}}{\Delta M_*} = \left(\frac{M_{\rm inf}}{M_{\rm II}}\right)^{x-1} - 1.4\frac{N_{\rm II} M_\odot}{\Delta M_*} \simeq 0.2, \quad \text{(A20)}$$

and the mass return rate per unit volume of the young evolving stellar population is given by

$$\dot{\rho}_{\rm II}(t) \simeq \frac{0.2}{\tau_{\rm II}} \int_0^t \dot{\rho_*}^+(t') e^{-(t-t')/\tau_{\rm II}} dt'. \quad \text{(A21)}$$

Finally, in the code we also compute the fiducial optical and UV luminosity per unit volume of the new stars as

$$\dot{E}_{\rm opt}(t) \equiv \frac{\epsilon_{\rm opt} c^2}{\tau_{\rm opt}} \int_0^t \dot{\rho_*}^+(t') e^{-(t-t')/\tau_{\rm opt}} dt', \quad \text{(A22)}$$

and

$$\dot{E}_{\rm UV}(t) \equiv \frac{\epsilon_{\rm UV} c^2}{\tau_{\rm UV}} \int_0^t \dot{\rho_*}^+(t') e^{-(t-t')/\tau_{\rm UV}} dt', \quad \text{(A23)}$$

respectively, where $\epsilon_{\rm opt} = 1.24 \times 10^{-3}$, $\epsilon_{\rm UV} = 8.65 \times 10^{-5}$, $\tau_{\rm opt} = 1.54 \times 10^8$ yr, and $\tau_{\rm UV} = 2.57 \times 10^6$ yr are the efficiency and characteristic time of optical and UV emission, respectively.

A4. Radiative Heating and Cooling

Compton heating and cooling, bremsstrahlung losses, line and recombination continuum heating and cooling, are taken into account.

A good approximation to the net gas energy change rate $\dot{E}$, valid for $T \gtrsim 10^4$ K (all quantities are expressed in cgs system) is given by

$$\dot{E} = n^2(S_1 + S_2 + S_3) \equiv H - C, \quad \text{(A24)}$$

where n is the hydrogen density (in number), and positive and negative terms are grouped together in the heating (H) and cooling (C) functions. The bremsstrahlung losses are given by

$$S_1 = -3.8 \times 10^{-27}\sqrt{T}, \quad \text{(A25)}$$

the Compton heating and cooling is given by

$$S_2 = 4.1 \times 10^{-35}(T_{\rm X} - T)\,\xi, \quad \text{(A26)}$$

where T_X is the Compton temperature, and finally the sum of photoionization heating, line and recombination continuum cooling is

$$S_3 = 10^{-23}\frac{a + b\,(\xi/\xi_0)^c}{1 + (\xi/\xi_0)^c}, \tag{A27}$$

where

$$a = -\frac{18}{e^{25(\log T - 4.35)^2}} - \frac{80}{e^{5.5(\log T - 5.2)^2}} - \frac{17}{e^{3.6(\log T - 6.5)^2}}, \tag{A28}$$

$$b = 1.7 \times 10^4\ T^{-0.7}, \tag{A29}$$

$$c = 1.1 - \frac{1.1}{e^{T/1.8\,10^5}} + \frac{4 \times 10^{15}}{T^4}, \tag{A30}$$

and

$$\xi_0 = \frac{1}{1.5\ T^{-0.5} + 1.5 \times 10^{12}\ T^{-2.5}} + \frac{4 \times 10^{10}}{T^2}\left[1 + \frac{80}{e^{(T-10^4)/1.5\,10^3}}\right]. \tag{A31}$$

Equations (A26) and (A27) depend on the ionization parameter

$$\xi \equiv \frac{L^{\rm eff}_{\rm BH,photo}(r)}{n(r)r^2}, \tag{A32}$$

where $L^{\rm eff}_{\rm BH,photo}(r)$ is the effective accretion luminosity at r, which is evaluated by numerically solving in each shell the balance equation

$$\frac{dL^{\rm eff}_{\rm BH,photo}(r)}{dr} = -4\pi r^2 H, \tag{A33}$$

with central boundary condition $L^{\rm eff}_{\rm BH,photo}(r = 0) = L_{\rm BH}(t)$ given by Equation (A46). The photoionization+Compton opacity associated with radiation absorption is then obtained

$$\kappa_{\rm photo} = -\frac{1}{\rho L^{\rm eff}_{\rm BH,photo}(r)}\frac{dL^{\rm eff}_{\rm BH,photo}(r)}{dr} = \frac{4\pi r^2 H(r)}{\rho(r) L^{\rm eff}_{\rm BH,photo}(r)}. \tag{A34}$$

Finally, the bolometric ISM luminosity is obtained from Equation (A24) as

$$L_{\rm r}(r) = 4\pi \int_0^r C r^2 dr. \tag{A35}$$

A5. Radiation Pressure

Radiation pressure due to *electron scattering* (where neither the photon numbers, nor their energy change) is computed as

$$(\nabla p_{\rm rad})_{\rm es} = -\frac{\kappa_{\rm es}\rho}{c}\frac{L_{\rm BH} + L_{\rm UV}(r) + L_{\rm opt}(r) + L_{\rm r}(r)}{4\pi r^2}, \tag{A36}$$

where $\kappa_{\rm es} = 0.35$ in cgs units, and from Equations (A22) and (A23)

$$L_{\rm UV}(r) = 4\pi \int_0^r \dot{E}_{\rm UV} r^2 dr, \quad L_{\rm opt}(r) = 4\pi \int_0^r \dot{E}_{\rm opt} r^2 dr. \tag{A37}$$

Note that all the luminosities used in Equation (A36) are unabsorbed.

The radiation pressure contribution due to dust opacity is given by

$$(\nabla p_{\rm rad})_{\rm dust} = -\frac{\kappa_{\rm UV}\rho}{c}\frac{L^{\rm eff}_{\rm BH,UV}(r) + L^{\rm eff}_{\rm UV}(r)}{4\pi r^2} - \frac{\kappa_{\rm opt}\rho}{c}\frac{L^{\rm eff}_{\rm BH,opt}(r) + L^{\rm eff}_{\rm opt}(r)}{4\pi r^2} - \frac{\kappa_{\rm IR}\rho}{c}\frac{L_{\rm IR}(r)}{4\pi r^2}, \tag{A38}$$

where

$$L_{\rm IR}(r) \equiv L^{\rm abs}_{\rm BH,UV}(r) + L^{\rm abs}_{\rm BH,opt}(r) + L^{\rm abs}_{\rm UV}(r) + L^{\rm abs}_{\rm opt}(r), \tag{A39}$$

is the infrared luminosity due to recycling of photons absorbed from the ISM, and we adopt as estimates for (cgs) opacity in three bands

$$\kappa_{\rm opt} = \frac{300}{1 + T/10^4}, \quad \kappa_{\rm UV} = 4\kappa_{\rm opt}, \quad \kappa_{\rm IR} = \frac{\kappa_{\rm opt}}{150}. \tag{A40}$$

At variance with electron scattering, the effective luminosities appearing in Equations (A38) and (A39) take into account absorption, and are obtained by numerically solving the two lowest spherically symmetric moment equations of radiative transfer in the Eddington approximation (e.g., Chandrasekhar 1960):

$$\frac{dL^{\rm eff}_{\rm UV}}{dr} = 4\pi r^2(\dot{E}_{\rm UV} - \kappa_{\rm UV}\rho J^{\rm eff}_{\rm UV}),$$
$$\frac{dL^{\rm eff}_{\rm opt}}{dr} = 4\pi r^2(\dot{E}_{\rm opt} - \kappa_{\rm opt}\rho J^{\rm eff}_{\rm opt}). \tag{A41}$$

$$\frac{dJ^{\rm eff}_{\rm UV}}{dr} = -\frac{3\kappa_{\rm UV}\rho L^{\rm eff}_{\rm UV}}{4\pi r^2}, \quad \frac{dJ^{\rm eff}_{\rm opt}}{dr} = -\frac{3\kappa_{\rm opt}\rho L^{\rm eff}_{\rm opt}}{4\pi r^2}. \tag{A42}$$

The central boundary conditions for stellar luminosities are $L^{\rm eff}_{\rm UV}(0) = L_{\rm d,UV}$, $L^{\rm eff}_{\rm opt}(0) = L_{\rm d,opt}$, $J^{\rm eff}_{\rm UV}(0) = L_{\rm d,UV}/16\pi^2 R_1^2$ and $J^{\rm eff}_{\rm opt}(0) = L_{\rm d,opt}/16\pi^2 R_1^2$. The effective accretion luminosities $L^{\rm eff}_{\rm BH,UV}$ and $L^{\rm eff}_{\rm BH,opt}$ are computed with two equations similar to Equation (A41), where the distributed source term is missing, $J = L^{\rm eff}_{\rm BH}/4\pi r^2$, and in the UV and optical bands $L^{\rm eff}_{\rm BH,UV}(0) = 0.2L_{\rm BH}(t)$ and $L^{\rm eff}_{\rm BH,opt}(0) = 0.1L_{\rm BH}(t)$, respectively.

The last contribution to radiation pressure comes from photoionization opacity,

$$(\nabla p_{\rm rad})_{\rm photo} = -\frac{\rho\kappa_{\rm photo}}{c}\frac{L^{\rm eff}_{\rm BH,photo}(r)}{4\pi r^2}. \tag{A43}$$

A6. The Circumnuclear Disk and the SMBH Accretion Luminosity

The circumnuclear disk, which is the repository of the gas inflowing at a rate $\dot{M}^{\rm eff}_1$ from the first active mesh point R_1 of the hydrodynamical grid, and which feeds the central SMBH at a rate $M_{\rm BH}$, contains at any time the mass gas $M_{\rm dg}$ and a total stellar mass $M_{\rm d*} = M_{\rm dl*} + M_{\rm dh*}$, which is divided among low and high-mass stars (with the division mass at 8 $M_\odot$). The disk also contains a mass $M_{\rm rem}$ of remnants from the earlier generations of evolved stars.

In the adopted scheme the accretion rate on the central SMBH is given by

$$\dot{M}_{\rm BH} = \frac{\dot{M}_{\rm fid}}{1 + \eta_{\rm d}}, \tag{A44}$$

where

$$\dot{M}_{\rm fid} \equiv \frac{M_{\rm dg}}{\tau_{\rm d}}, \quad \eta_{\rm d} \equiv \frac{\dot{M}_{\rm fid}}{2\dot{M}_{\rm Edd}}, \quad \dot{M}_{\rm Edd} \equiv \frac{L_{\rm Edd}}{\epsilon_0 c^2} \tag{A45}$$

are the fiducial depletion rate of gas from the circumnuclear disk, its normalized value, and the Eddington mass accretion rate, respectively. The reference radiative efficiency ϵ_0 is defined in Equation (A47). Equations (A44) and (A45) are designed to guarantee that when $\eta_{\rm d} \ll 1$ the gas is accreted onto the central SMBH at the rate $\dot{M}_{\rm fid}$, while $\dot{M}_{\rm BH} = 2\dot{M}_{\rm Edd}$ for $\eta_{\rm d} \gg 1$ (i.e., we allow for possible moderate super-Eddington accretion; note, however, that outside the first grid point R_1 the flow accretion rate is limited in a self-consistent way by feedback effects). From Equation (A44), we calculate the instantaneous bolometric accretion luminosity as

$$L_{\rm BH} = \epsilon_{\rm EM}\, \dot{M}_{\rm BH}\, c^2, \tag{A46}$$

where

$$\epsilon_{\rm EM} = \epsilon_0 \frac{A\dot{m}}{1 + A\dot{m}}, \quad \dot{m} \equiv \frac{\dot{M}_{\rm BH}}{\dot{M}_{\rm Edd}}, \tag{A47}$$

and A is a free parameter so that $\epsilon_{\rm EM} \sim \epsilon_0 A\dot{m}$ for $\dot{m} \ll A^{-1}$. In our simulations, we fix $A = 100$, and we introduce the normalized accretion luminosity

$$l \equiv \frac{L_{\rm BH}}{L_{\rm Edd}} = \frac{A\dot{m}^2}{1 + A\dot{m}}, \tag{A48}$$

where the last expression derives from the ADAF phenomenological description.

There are a few lag times in our problem which are expressed as follows. The first is the instantaneous disk lag time, appearing in Equation (A45):

$$\tau_{\rm d} \equiv \frac{2\pi}{\alpha}\sqrt{\frac{R_{\rm d}^3}{GM_{\rm BH}}}, \tag{A49}$$

where $\alpha \simeq 10^{-2}$–10^{-1} is the disk viscosity coefficient, and $R_{\rm d}$ and $M_{\rm BH}$ are the instantaneous values of the fiducial radius of the circumnuclear disk and the mass of the central SMBH. We use the scaling predicted by thin-disk theory

$$R_{\rm d}(t) = f_d R_1 \times \left(\frac{M_{\rm BH}}{M_{\rm BH0}}\right)^{2/3}, \tag{A50}$$

where $M_{\rm BH0}$ is the central SMBH mass at the beginning of the simulation. We assume $f_d = 0.4$, so that $R_{\rm d}(0) \simeq 2$ pc for an initial SMBH mass of $\simeq 10^8\, M_\odot$.

The second characteristic time is the instantaneous infall lag time from R_1 to the disk:

$$\tau_{\rm i} = \frac{R_1}{v_{\rm ff}}, \quad v_{\rm ff} \equiv \sqrt{\frac{2GM_{\rm BH}}{R_1}}, \tag{A51}$$

so that the effective rate at which gas accretes on the disk is obtained by solving the differential equation

$$\frac{d\dot{M}_1^{\rm eff}}{dt} = \frac{\dot{M}_1 - \dot{M}_1^{\rm eff}}{\tau_{\rm i}}, \tag{A52}$$

where $\dot{M}_1$ is the instantaneous rate at which gas flows through the first active grid point.[6] It follows that when $\dot{M}_1$ provided by hydrodynamics drops to zero the circumnuclear disk experiences a fueling declining exponentially with time.

The disk total gas mass $M_{\rm dg}$ is not only the source of SMBH accretion, but also of star formation in the disk: we assume that a fraction of $M_{\rm dg}$ is converted into stars at a rate $\eta_* \dot{M}_{\rm fid}$ (where $\eta_* \simeq 10 M_{\rm dg}/M_{\rm BH}$), and that another fraction of $M_{\rm dg}$ is lost as a *disk wind* and as a *jet* at instantaneous rates given by $\eta_{\rm w}\dot{M}_{\rm BH}$ and $\eta_{\rm j}\dot{M}_{\rm BH}$, so that the equation for the gas mass in the disk is

$$\frac{dM_{\rm dg}}{dt} = \dot{M}_1^{\rm eff} - (1 + \eta_{\rm w} + \eta_{\rm j})\dot{M}_{\rm BH} - \eta_* \dot{M}_{\rm fid}. \tag{A53}$$

The stars formed in the disk are described separately as a function of their mass, i.e., high-mass stars ($M > M_{\rm II} = 8\, M_\odot$) produce a total disk mass $M_{\rm dh*}$, and low-mass stars ($M_{\rm inf} < M < M_{\rm II}$) contribute to a disk mass $M_{\rm dl*}$ according to the equations

$$\frac{dM_{\rm dl*}}{dt} = (1-f_{\rm h})\eta_* \dot{M}_{\rm fid} - \frac{M_{\rm dl*}}{\tau_{*\rm l}}; \quad \frac{dM_{\rm dh*}}{dt} = f_{\rm h}\eta_* \dot{M}_{\rm fid} - \frac{M_{\rm dh*}}{\tau_{*\rm h}}. \tag{A54}$$

For the characteristic evolutionary times, we adopt $\tau_{*\rm l} = \tau_{\rm opt}$ and $\tau_{*\rm h} = \tau_{\rm II}$, while we assume $f_{\rm h} = 0.5$, corresponding to a top-heavy Salpeter-like initial mass function of slope $x \simeq 1.16$ and minimum mass $M_{\rm inf} = 0.1\, M_\odot$. The associated optical ($L_{\rm d,opt}$) and UV ($L_{\rm d,UV}$) luminosities of the stellar disk are calculated following the scheme described in Ciotti & Ostriker (2007). Finally, stellar remnants mass in the disk evolves as

$$\frac{dM_{\rm rem}}{dt} = f_{\rm rem,l}\frac{M_{\rm dl*}}{\tau_{*\rm l}} + f_{\rm rem,h}\frac{M_{\rm dh*}}{\tau_{*\rm h}}, \tag{A55}$$

where $f_{\rm rem,l} = 0.2$ and $f_{\rm rem,h} = 0.09$.

The equation for the mass loss associated with the disk wind is

$$\frac{dM_{\rm dw}}{dt} = \eta_{\rm w}\dot{M}_{\rm BH} + (1-f_{\rm rem,l})\frac{M_{\rm dl*}}{\tau_{*\rm l}} + (1-f_{\rm rem,h})\frac{M_{\rm dh*}}{\tau_{*\rm h}}: \tag{A56}$$

the first term is a mass loss driven as a wind by the central SMBH, and the second and third are from high-mass and low-mass stars in the central disk.

We explore two different classes of models, that we call *Type A* and *Type B*, with

$$\eta_{\rm w} \equiv \begin{cases} 2, & \text{(Type A)} \\ \dfrac{3\eta_{\rm w}^{\rm M}}{4}\dfrac{l}{1 + 0.25l}, & \text{(Type B).} \end{cases} \tag{A57}$$

We also consider another mass component ejected by disk, i.e., a nuclear jet with instantaneous mass flow

$$\frac{dM_{\rm j}}{dt} = \eta_{\rm j}\dot{M}_{\rm BH}, \quad \eta_{\rm j} = \frac{0.2}{(1 + 100l)^4}, \tag{A58}$$

so that the mass ejected by the jet is always negligible with respect to the wind mass loss in Type A models, while it is slightly dominant over the wind in Type B models at low-luminosity ratios. In the code, all the equations presented in this section are integrated numerically with a first-order finite difference scheme.

A7. The Mechanical Feedback Treatment

We now discuss how the kinetic energy, momentum, and mass of the broad-line region (BLR) wind are transferred to the ISM.

[6] $\dot{M}_1$ is taken positive in case of accretion and zero in case of outflow at R_1.

The fiducial instantaneous mechanical luminosity of the disk wind is given by

$$L_{\rm dw} = \epsilon_{\rm w}\dot{M}_{\rm BH}c^2 + \epsilon_{\rm II}c^2(1 - f_{\rm rem,h})\frac{M_{\rm dh*}}{\tau_{*\rm h}}, \quad \text{(A59)}$$

where $\epsilon_{\rm w}$ is the mechanical efficiency of the wind, and the second term describes the energetic associated with the SN II explosions of the high-mass stars in the circumnuclear disk. In analogy with Equation (A57), we assume

$$\epsilon_{\rm w} \equiv \begin{cases} \epsilon_{\rm w}^{\rm M}, & \text{(Type A)} \\ \dfrac{3\epsilon_{\rm w}^{\rm M}}{4}\dfrac{l}{1+0.25l}, & \text{(Type B).} \end{cases} \quad \text{(A60)}$$

In Type A models, we explore the range $3\,10^{-5} \leqslant \epsilon_{\rm w}^{\rm M} \leqslant 5\,10^{-3}$. In Type B models, where the wind efficiency is a function of the normalized accretion luminosity, $\epsilon_{\rm w}^{\rm M}$ is the maximum possible value (reached for $l = 2$). In both cases, the instantaneous disk wind velocity is given by

$$v_{\rm w} \equiv \sqrt{\frac{2L_{\rm dw}}{\dot{M}_{\rm dw}}} \simeq \sqrt{\frac{2\epsilon_{\rm w}}{\eta_{\rm w}}}c, \quad \text{(A61)}$$

where the last expression neglects the mass return contribution of massive stars in the circumnuclear disk. In Type A models, $v_{\rm w}$ is in the range 2×10^3–2×10^4 km s^{-1} (as a function of the specific assumed value for $\epsilon_{\rm w}$), in agreement with observations of BLRs. For the same reasons, in Type B models we require $v_{\rm w} = 10^4$ km s^{-1}, so that $\eta_{\rm w}^{\rm M}$ and $\epsilon_{\rm w}^{\rm M}$ are linked by the relation

$$\eta_{\rm w}^{\rm M} = 1800\epsilon_{\rm w}^{\rm M}. \quad \text{(A62)}$$

In analogy with the wind component, the instantaneous jet mechanical luminosity is written as

$$L_{\rm j} = \epsilon_{\rm j}\dot{M}_{\rm BH}c^2, \quad \epsilon_{\rm j} = \frac{0.0125}{(1+400l)^4}, \quad \text{(A63)}$$

and the jet velocity is given by

$$v_{\rm j} \equiv \sqrt{\frac{2L_{\rm j}}{\dot{M}_{\rm j}}} = \sqrt{\frac{2\epsilon_{\rm j}}{\eta_{\rm j}}}\,c, \quad \text{(A64)}$$

which, for our chosen parameterization gives high but subrelativistic jet velocity of $v_{\rm j}/c \simeq 10^{-1.65}$ for $l \gtrsim 0.1$. Finally, the wind and jet momentum are defined as

$$m_{\rm j} \equiv \dot{M}_{\rm j}v_{\rm j}; \quad m_{\rm w} \equiv \dot{M}_{\rm dw}v_{\rm w}. \quad \text{(A65)}$$

We now illustrate how we distribute the mechanical feedback over the galaxy ISM. First, we introduce the instantaneous wind and jet lag times

$$\tau_{\rm wj} \equiv \frac{R_1}{v_{\rm wj}} \quad \text{(A66)}$$

from the center to the first active grid point R_1 (where the subscript indicates the specific component—disk wind or nuclear jet—considered), and at each time step we compute the time-lagged values for mass, momentum, and kinetic energy at R_1 by solving the differential equation

$$\frac{dX_l}{dt} = \frac{X - X_l}{\tau_{\rm wj}}, \quad \text{(A67)}$$

where X_l is the generic lagged variable associated with the instantaneous unlagged value X. Outside R_1 we then distribute mass, momentum and kinetic energy over the hydrodynamical grid (outside R_1), by integrating numerically the phenomenological differential equation

$$\frac{\partial \ln Y_{\rm wj}}{\partial \ln r} = -\frac{P_{\rm ISM}(r)}{P_{\rm wj}(r)} - \frac{r}{v_{\rm wj}}\frac{\partial \ln Y_{\rm wj}}{\partial t}, \quad \text{(A68)}$$

where $Y_{\rm wj}$ is the mass, momentum, and energy of the disk wind/jet component at distance r from the center, $P_{\rm wj}(r)$ is the local wind/jet pressure, and for each quantity $Y(R_1) = X_l$. In this paper, we restrict to simulations where the time derivative is neglected. In practice, we first integrate Equation (A68) for the wind/jet pressure, i.e.,

$$P_{\rm wj} = \frac{Y_{\rm wj}}{2\Delta\Omega_{\rm wj}r^2}, \quad \text{(A69)}$$

where $Y_{\rm wj}$ is the effective wind/jet momentum crossing the shell of radius r, so that Equation (A68) is a nonlinear differential equation for $Y_{\rm wj}$. Once the equation is integrated, the radial behavior of $P_{\rm wj}$ and the right-hand side of Equation (A68) are known over the whole grid, and the equation can be integrated for mass and energy.

The solid angle in the denominator of Equation (A69) is the opening angle of the wind and of the jet, and the factor of 2 accounts for the biconical nature of the flow. While for the jet we assumed in all the simulations the fiducial value $\Delta\Omega_{\rm j} = 2.5 \times 10^{-2}$, for the wind case we adopt

$$\Delta\Omega_{\rm w} = \begin{cases} \pi & \text{(Type A)} \\ \pi\,\min(\sqrt{l^2 + a^2}, 1), & \text{(Type B),} \end{cases} \quad \text{(A70)}$$

where case B is designed to mimic the behavior found in radiation driven winds: higher luminosity corresponds to a larger opening angles. The constant inside the square root is fixed to $a = \Delta\Omega_{\rm j}/\pi$, so that for small values of accretion luminosity the wind opening angle coincides with the jet opening angle. Finally, note that the almost linear dependence of $\Delta\Omega_{\rm w}$ on l for $l > a$ assumes that the linear opening angle depends on $\sqrt{l}$ for this regime.

To implement numerically the mechanical feedback terms, we finally compute the nuclear wind mass, momentum, and kinetic energy per unit volume deposited in each shell as

$$\text{Source}_{\rm wj} = \frac{3}{4\pi}\frac{Y_{\rm wj}(R_i) - Y_{\rm wj}(R_{i+1})}{R_{i+1}^3 - R_i^3} \quad \text{(A71)}$$

and we add them (only for the wind component) to the right-hand side of Equations (A1)–(A3).

REFERENCES

Angeletti, L., & Giannone, P. 2003, A&A, 403, 449
Ballero, S. K., Matteucci, F., Ciotti, L., Calura, F., & Padovani, P. 2008, A&A, 478, 335
Batcheldor, D., Tadhunter, C., Holt, J., Morganti, R., O'Dea, C. P., Axon, D. J., & Koekemoer, A. 2007, ApJ, 661, 70
Begelman, M. C., & Nath, B. B. 2005, MNRAS, 361, 1387
Binney, J., & Tabor, G. 1995, MNRAS, 276, 663
Blandford, R. 2001, in Proc. IAU Symp. 205, Galaxies and their Constituents at the Highest Angular Resolutions, ed. R. T. Schilizzi (San Francisco, CA: ASP), 10
Boyle, B. J., & Terlevich, R. J. 1998, MNRAS, 293, L49
Carollo, C. M., Danziger, I. J., & Buson, L. 1993, MNRAS, 265, 553

Cattaneo, A., Blaizot, J., Devriendt, J., & Guiderdoni, B. 2005, MNRAS, 364, 407
Cattaneo, A., et al. 2007, MNRAS, 377, 63
Cattaneo, A., et al. 2009, Nature, 460, 213
Cavaliere, A., Giallongo, E., Vagnetti, F., & Messina, A. 1983, ApJ, 269, 57
Cavaliere, A., Lapi, A., & Menci, N. 2002, ApJ, 581, L1
Chandran, B. D. G., & Rasera, Y. 2007, ApJ, 671, 1413
Chandrasekhar, S. 1960, Radiative Transfer (New York: Dover)
Chatterjee, S., di Matteo, T., Kosowsky, A., & Pelupessy, I. 2008, MNRAS, 390, 535
Ciotti, L. 2009, Nuovo Cimento Riv. Ser., 32, 1
Ciotti, L., D'Ercole, A., Pellegrini, S., & Renzini, A. 1991, ApJ, 376, 380
Ciotti, L., Morganti, L., & de Zeeuw, P. T. 2009a, MNRAS, 393, 491
Ciotti, L., & Ostriker, J. P. 1997, ApJ, 487, L105
Ciotti, L., & Ostriker, J. P. 2001, ApJ, 551, 131
Ciotti, L., & Ostriker, J. P. 2007, ApJ, 665, 1038
Ciotti, L., Ostriker, J. P., & Proga, D. 2009b, ApJ, 699, 89
Crenshaw, D. M., Kraemer, S. B., & George, I. M. 2003, ARA&A, 41, 117
Croton, D. J., et al. 2006, MNRAS, 365, 11
David, L. P., Jones, C., Forman, W., Vargas, I. M., & Nulsen, P. 2006, ApJ, 653, 207
Davies, R. I., Mueller Sánchez, F., Genzel, R., Tacconi, L. J., Hicks, E. K. S., Friedrich, S., & Sternberg, A. 2007, ApJ, 671, 1388
D'Ercole, A., Recchi, S., & Ciotti, L. 2000, ApJ, 533, 799
Donas, J., et al. 2007, ApJS, 173, 597
Drory, N., & Alvarez, M. 2008, ApJ, 680, 41
Elmegreen, B. G., Bournaud, F., & Elmegreen, D. M. 2008, ApJ, 684, 829
Elvis, M. 2000, ApJ, 545, 63
Elvis, M. 2006, Mem. Soc. Astron. Ital., 77, 573
Elvis, M., et al. 1994, ApJS, 95, 1
Fabian, A. C. 1999, MNRAS, 308, L39
Fabian, A. C., Celotti, A., & Erlund, M. C. 2006, MNRAS, 373, L16
Ferrarese, L. 2002, ApJ, 578, 90
Ferrarese, L., & Merritt, D. 2000, ApJ, 539, L9
Friaca, A. C. S., & Terlevich, R. J. 1998, MNRAS, 298, 399
Fu, H., & Stockton, A. 2009, ApJ, 690, 953
Gebhardt, K., et al. 2000, ApJ, 539, L13
Gibson, B. K. 1996, ApJ, 468, 167
Graham, A. W., Erwin, P., Caon, N., & Trujillo, I. 2001, ApJ, 563, L11
Granato, G. L., De Zotti, G., Silva, L., Bressan, A., & Danese, L. 2004, ApJ, 600, 580
Grogin, N. A., et al. 2005, ApJ, 627, L97
Haiman, Z., Ciotti, L., & Ostriker, J. P. 2004, ApJ, 606, 763
Hardee, P. 2008, J. Phys. Conf. Ser., 131, 012052
Häring, N., & Rix, H.-W. 2004, ApJ, 604, L89
Heckman, T. M. 2009, in Astrophysics of The Next Decade, ed. H. A. Thronson, M. Stiavelli, & A. G. G. M. Tielens (Dordrecht: Springer), 335
Ho, L. C. 2008, ARA&A, 46, 475
Hopkins, P. F., Hernquist, L., Cox, T. J., & Kereš, D. 2008, ApJS, 175, 356
Hopkins, P. F., Hernquist, L., Martini, P., Cox, T. J., Robertson, B., Di Matteo, T., & Springel, V. 2005, ApJ, 625, L71
Humphrey, P. J., Buote, D. A., Gastaldello, F., Zappacosta, L., Bullock, J. S., Brighenti, F., & Mathews, W. G. 2006, ApJ, 646, 899
Jaffe, W. 1983, MNRAS, 202, 995
Jogee, S. 2006, in Physics of Active Galactic Nuclei at all Scales, Lecture Notes in Physics, Vol. 693, ed. D. Alloin (New York: Springer), 143
Johansson, P. H., Naab, T., & Burkert, A. 2009, ApJ, 690, 802
Kang, X., van den Bosch, F. C., & Pasquali, A. 2007, MNRAS, 381, 389
Kaviraj, S., et al. 2007, ApJS, 173, 619
Kawaguchi, T. 2003, ApJ, 593, 69
Kawata, D., & Gibson, B. K. 2005, MNRAS, 358, L16
Khalatyan, A., Cattaneo, A., Schramm, M., Gottlöber, S., Steinmetz, M., & Wisotzki, L. 2008, MNRAS, 387, 13
Kim, D.-W., & Fabbiano, G. 2004, ApJ, 611, 846
Kim, M., Ho, L. C., Peng, C. Y., Barth, A. J., Im, M., Martini, P., & Nelson, C. H. 2008, ApJ, 687, 767
King, A. 2003, ApJ, 596, L27
King, A. 2005, ApJ, 635, L121
King, A. R., & Pounds, K. A. 2003, MNRAS, 345, 657
Kirkman, D., & Tytler, D. 2008, MNRAS, 391, 1457
Kisaka, S., Kojima, Y., & Otani, Y. 2008, MNRAS, 390, 814
Königl, A. 2006, Mem. Soc. Astron. Ital., 77, 598
Kormendy, J., Fisher, D. B., Cornell, M. E., & Bender, R. 2009, ApJS, 182, 216
Kormendy, J., & Richstone, D. 1995, ARA&A, 33, 581
Krolik, J. H. 1999, in Active Galactic Nuclei: From the Central Black Hole to the Galactic Environment, ed. Julian H. Krolik (Princeton, NJ: Princeton Univ. Press)
Krongold, Y., Nicastro, F., Elvis, M., Brickhouse, N., Jiménez-Bailón, E., Binette, L., & Mathur, S. 2008, RevMexAA Conf. Ser., 27, 123
Kurosawa, R., & Proga, D. 2009, ApJ, 693, 1929
Lagos, C. D. P., Cora, S. A., & Padilla, N. D. 2008, MNRAS, 388, 587
Letawe, Y., Magain, P., Letawe, G., Courbin, F., & Hutsemékers, D. 2008, ApJ, 679, 967
Levine, R., & Gnedin, N. Y. 2005, ApJ, 632, 727
Li, C., Kauffmann, G., Heckman, T. M., White, S. D. M., & Jing, Y. P. 2008, MNRAS, 385, 1915
Magorrian, J., et al. 1998, AJ, 115, 2285
Maller, A. H., Katz, N., Kereš, D., Davé, R., & Weinberg, D. H. 2006, ApJ, 647, 763
Marconi, A., & Hunt, L. K. 2003, ApJ, 589, L21
Martini, P. 2004, in Coevolution of Black Holes and Galaxies, ed. L. C. Ho (Cambridge: Cambridge Univ. Press), 169
Matteucci, F., & Padovani, P. 1993, ApJ, 419, 485
Max, C. E., Canalizo, G., & de Vries, W. H. 2007, Science, 316, 1877
Menci, N., Fiore, F., Puccetti, S., & Cavaliere, A. 2008, ApJ, 686, 219
Merloni, A., & Heinz, S. 2008, MNRAS, 388, 1011
Miller, L. 2007, in ASP Conf. Ser. 379, Cosmic Frontiers, ed. N. Metcalfe & T. Shanks (San Francisco, CA: ASP), 194
Monaco, P., Fontanot, F., & Taffoni, G. 2007, MNRAS, 375, 1189
Müller Sánchez, F., Davies, R. I., Genzel, R., Tacconi, L. J., Eisenhauer, F., Hicks, E. K. S., Friedrich, S., & Sternberg, A. 2009, ApJ, 691, 749
Murray, N., Quataert, E., & Thompson, T. A. 2005, ApJ, 618, 569
Narayan, R., & Quataert, E. 2005, Science, 307, 77
Netzer, H., & Trakhtenbrot, B. 2007, ApJ, 654, 754
Nulsen, P. E. J., & Fabian, A. C. 2000, MNRAS, 311, 346
O'Sullivan, E., Forbes, D. A., & Ponman, T. J. 2001, MNRAS, 328, 461
Padovani, P., & Matteucci, F. 1993, ApJ, 416, 26
Pellegrini, S., Ciotti, L., & Ostriker, J. P. 2009, Adv. Space Res., 44, 340
Pipino, A., Silk, J., & Matteucci, F. 2009, MNRAS, 392, 475
Pope, E. C. D. 2009, MNRAS, 395, 2317
Proga, D. 2005, ApJ, 630, L9
Proga, D. 2007, ApJ, 661, 693
Proga, D., Ostriker, J. P., & Kurosawa, R. 2008, ApJ, 676, 101
Quataert, E. 2004, ApJ, 613, 322
Quataert, E., & Narayan, R. 2000, ApJ, 528, 236
Rees, M. J. 1984, ARA&A, 22, 471
Robertson, B., Hernquist, L., Cox, T. J., Di Matteo, T., Hopkins, P. F., Martini, P., & Springel, V. 2006, ApJ, 641, 90
Sánchez-Blázquez, P., Forbes, D. A., Strader, J., Brodie, J., & Proctor, R. 2007, MNRAS, 377, 759
Sazonov, S. Y., Ostriker, J. P., & Sunyaev, R. A. 2004, MNRAS, 347, 144
Sazonov, S. Y., Ostriker, J. P., Ciotti, L., & Sunyaev, R. A. 2005, MNRAS, 358, 168
Scannapieco, E., & Oh, S. P. 2004, ApJ, 608, 62
Scannapieco, E., Silk, J., & Bouwens, R. 2005, ApJ, 635, L13
Scannapieco, E., Thacker, R. J., & Couchman, H. M. P. 2008, ApJ, 678, 674
Shankar, F., Weinberg, D. H., & Miralda Escudé, J. 2009, ApJ, 690, 20
Shlosman, I., Begelman, M. C., & Frank, J. 1990, Nature, 345, 679
Shull, J. M. 1983, ApJ, 264, 446
Silk, J. 2005, MNRAS, 364, 1337
Silk, J., & Rees, M. J. 1998, A&A, 331, L1
Soria, R., Fabbiano, G., Graham, A. W., Baldi, A., Elvis, M., Jerjen, H., Pellegrini, S., & Siemiginowska, A. 2006a, ApJ, 640, 126
Soria, R., Graham, A. W., Fabbiano, G., Baldi, A., Elvis, M., Jerjen, H., Pellegrini, S., & Siemiginowska, A. 2006b, ApJ, 640, 143
Soltan, A. 1982, MNRAS, 200, 115
Spolaor, M., Proctor, R. N., Forbes, D. A., & Couch, W. J. 2009, ApJ, 691, L138
Springel, V., Di Matteo, T., & Hernquist, L. 2005a, ApJ, 620, L79
Springel, V., Di Matteo, T., & Hernquist, L. 2005b, MNRAS, 361, 776
Tabor, G., & Binney, J. 1993, MNRAS, 263, 323
Tan, J. C., Beuther, H., Walter, F., & Blackman, E. G. 2008, ApJ, 689, 775
Tan, J. C., & Blackman, E. G. 2005, MNRAS, 362, 983
Tecza, M., Genzel, R., Tacconi, L. J., Anders, S., Tacconi-Garman, L. E., & Thatte, N. 2000, ApJ, 537, 178
Thacker, R. J., Scannapieco, E., & Couchman, H. M. P. 2006, ApJ, 653, 86
Veilleux, S., Cecil, G., & Bland-Hawthorn, J. 2005, ARA&A, 43, 769
Yi, S. K., Kaviraj, S., Schawinski, K., & Khochfar, S. 2007, in EAS Publ. Ser. 24, CRAL-2006. Chemodynamics: From First Stars to Local Galaxies, ed. E. Emsellem et al. (Les Ulis: EDP Sciences), 73
Yu, Q., & Tremaine, S. 2002, MNRAS, 335, 965